THERMAL CHARACTERIZATION OF AUSTENITE STAINLESS STEEL (304) AND CNT FILMS OF VARYING THICKNESS USING MICROPIPETTE THERMAL SENSORS

Ashesh Dangol

Thesis Prepared for the Degree of

MASTER OF SCIENCE

UNIVERSITY OF NORTH TEXAS

May 2013

APPROVED:

Tae-Youl Choi, Major Professor
Mihai G. Burzo, Committee Member
Jiangtao Cheng, Committee Member
Yong X. Tao, Chair of the Department of Mechanical and Energy Engineering
Xun Yu, Graduate Program Coordinator
Costas Tsatsoulis, Dean of the College of Engineering
Mark Wardell, Dean of the Toulouse Graduate School

Dangol, Ashesh. Thermal characterization of austenite stainless steel (304) and CNT films of varying thickness using micropipette thermal sensors. Master of Science (Mechanical and Energy Engineering), May 2013, 77 pp., 11 tables, 30 illustrations, chapter references.

Thermal transport behavior of austenite stainless steel stripe (304) and the carbon nano-tubes (CNTs) films of varying thickness are studied using a micropipette thermal sensor. Micropipette sensors of various tip sizes were fabricated and tested for the sensitivity and reliability. The sensitivity deviated by 0.11 for a batch of pipette coated under same physical vapor deposition (PVD) setting without being affected by a tip size. Annealing, rubber coating and the vertical landing test of the pipette sensor proved to be promising in increasing the reliability and durability of the pipette sensors. A micro stripe (80μm × 6μm × 0.6μm) of stainless steel, fabricated using focused ion beam (FIB) machining, was characterized whose thermal conductivity was determined to be 14.9 W/m-K at room temperature. Similarly, the thermal characterization of CNT films showed the decreasing tendency in the thermal transport behavior with the increase in the film thickness.

ACKNOWLEDGEMENTS

I wish to thank, first and foremost, my major Professor Dr. Tae-Youl Choi for all his support, guidance and help throughout my entire academic career at UNT. As an advisor he has taken me to the path where I would have never thought and dreamed about. I really do appreciate his patience and confidence towards me. I am thankful for all his comments, instructions and suggestions throughout the entire research work. His persistent motivation and directions have made this thesis possible and let me be where I stand today.

I would like to thank my committee members, Dr. Cheng and Dr. Burzo, for all their valuable comments and suggestions on my thesis work.

I share the credit of my work with my laboratory mates Dr. Kyungmin Lee (Daniel) and Ramesh Shrestha for all their support and letting me believe that I can get the job done. Their persistent help and direction in overcoming solutions to simple, yet complicated, problems had made this work possible. All the simulation and Focused ion Beam work has been directed by Dr. Lee, whereas, Ramesh has been a guide throughout the research period from the start to the end. Simply, if they weren't there I would have never accomplished my destiny.

Lastly, I would like to thank the entire faculty member and staff of MEEN-UNT for their help and cooperation throughout my stay at UNT. I would also like to take a moment to thank all my classmates who been there influencing me directly and indirectly throughout my stay at UNT.

TABLE OF CONTENTS

Page

LIST OF TABLES

Page

LIST OF ILLUSTRATIONS

Page

LIST OF ABBREVIATIONS

A	Surface area
AC	Alternative current
AFM	Atomic force microscope
CCD	Charge couple device
CNTs	Carbon nanotubes
D	Diameter of cylinder
DC	Direct current
dT	Temperature difference
dV	Open circuit voltage
E	Energy of an electron
e	Emissivity of an object
emf	Electro motive force
FIB	Focused ion beam
G	Acceleration due to gravity
Ga	Gallium
GIS	Gas injection system
Gr_x	Grashof number
h	Convective heat transfer coefficient
ID	Inner diameter
k	Thermal conductivity
K	Boltzmann constant
L	Length of cylinder

MEMS	Micro electro-mechanical systems
ND	Neutral density
NEMS	Nano electro-mechanical systems
Ni	Nickel
Nu_x	Nusselt number
OD	Outer diameter
P	Radiated energy
P_{abs}	Absorbed power of infrared radiation
Pr	Prandtl number
PVD	Physical vapor deposition
$\dot{Q}$	Heat flow
Ra_x	Rayleigh number
r_1, r_2	Radial positions
S	Thermoelectric power
S_v	Seebeck voltage
SEM	Scanning electron microscope
SS 304	Stainless steel 304
Sn	Tin
SWNTs	Single walled carbon nanotubes
S_1, S_2	Seebeck coefficient
T	Temperature of hot object
T_c	Temperature of the surrounding
TEM	Transmission electron microscope

T_f	Average fluid temperature
T_s	Surface temperature of sample
T_1, T_2	Temperature at radial position
x	Characteristic length
XRD	X-ray diffraction
XPS	X-ray photoelectron spectroscopy
A	Thermal diffusivity
B	Coefficient of volumetric expansion
σ	Stefan-Boltzmann constant
v	Kinematic viscosity
q''	Heat flux
∇T	Temperature gradient
Z	Fermi energy
λ	Mean free path of an electron

CHAPTER 1

INTRODUCTION

The 21st century is advancing towards the micro and nano scale. We can see the rapid reduction in the size of the electronic devices, and the integrated micro / nano electro-mechanical systems (MEMS and NEMS) [1]. The most common example would be the size of the computer then and now. The first computer was almost the size of the desk but today it is not the same. Similarly, transistors have replaced the vacuum tube which are smaller in sizes, and are also efficient and flexible to be used with the integrated circuits. Looking at the trend we can see the future with devices smaller than what we have today. This provides the need for the advancement of the scientific research in the field of micro / nano technology. While designing micro-electronic device, a particular issue that needs to be addressed is the change in thermal transport properties of the components [2]. In order to control the performance and stability of microelectronic devices it is necessary to understand the thermal behavior in detail [2].

Thermal conductivity is an intrinsic property of a material which measures the ability of materials to transport the heat energy. It can be defined as the quantity of heat energy transmitted per unit distance per unit temperature change over that distance in the direction of heat transfer. It is an important aspect in characterizing material performance. The thermal transport properties of the materials can impact the safety, reliability and performance of electronic and electro-optical devices. So, thermal characterization of thin films and micro strips are areas of interest which can help us understand the thermal transport phenomena in the micro / nano scale. One way to characterize them more precisely and accurately in micro level is through micro-level

thermal sensing technique which has been used for the research and study of the materials in this thesis.

Austenite stainless steel 304 (SS 304) is an important metal which are used to build nuclear reactors. They separate the reactor from the environment. Due to the continuous reaction inside the reactor there is high dose of ion irradiation and high temperature rise. Because of this irradiation the thermal properties of the stainless steel cladding are changing with time. The effect of these irradiations is seen even in the grain boundaries. So, the study of the effect of grain level boundaries, ion irradiation, and high temperature on the thermal property of the stainless steel will help to develop proper simulation protocols to improve the prediction capabilities in nuclear reactor model. In an effort to characterize the thermal properties at the micro scale I measure the thermal conductivity of the austenite stainless steel at micro level and compare with the literature values and simulation results.

Carbon nanotubes (CNTs) are the allotropes of carbon with cylindrical nanostructure. They have been constructed with length to diameter ratio of up to 132000000:1 which is significantly larger compared to other materials [3]. The small dimensions, strength and the remarkable electrical and physical properties of these structures make them a very unique material with a whole range of promising applications [4]. These properties are of importance in the field of nanotechnology, electronics, optoelectronics, biomedical, energy, optics, and other field of materials science and technology. They have enormous theoretical possibilities which make them the good research subject. There is potential application of CNTs in vacuum microelectronics like prototype electron emission devices based on carbon. CNTs are

also considered for energy production and storage because of its small dimensions, smooth surface topology, and perfect surface specificity. Electrochemical intercalation of CNTs with lithium and hydrogen storage is an example of CNTs application in energy storage [4]. The characteristics extremely small size, high conductivity, high mechanical strength and flexibility might make CNTs an indispensable in their use as nanoprobes , and these probes can be used for various application like high resolution imaging, nano-lithography, nanoelectrodes, drug delivery, sensors and field emitters [4]. Thin films of single walled carbon nanotubes (SWNTs) have their outstanding performance in gas and biosensing [5,6] as a transparent conducting coating for large area flexible optoelectronics [7-11], and as the thermal interface layer for heat dissipation in high density electronic packaging [12]. Other future expectation from CNTs are space elevator, faster computer chips, better solar cells, cancer treatment, thinner televisions, better capacitors that replaces batteries, flexible displays, bone healing, body armor, faster flywheels etc. We can say that we are looking tomorrow's technology with CNTs. So, in order to be able to use them efficiently and effectively the thermal characterization of CNTs at nano scale will help to get the detailed information on the behavior of CNTs which would definitely benefit the ongoing researches for building tomorrow's world with CNTs.

The characterization of the materials at a micro / nano scale is made possible with the help of different equipments like atomic force microscope (AFM), scanning electron microscope (SEM), transmission electron microscope (TEM), auger scanning nanoprobe, x-ray photoelectron spectroscopy (XRD), x-ray diffraction (XRD), focused ion beam (FIB), Raman spectrometer, profilometer, etc. Particularly, for this research

SEM and profilometer are used for characterization, and FIB is used for fabrication of micro stripe and characterization. For the thermal conductivity measurement a laser point source is employed for heating and the advance high sensitive micropipette thermal sensor (of around ~1µm diameter) for measuring the temperature at different position on the surface of stainless steel stripe and CNT films.

In this thesis, the fabrication of a micro scale stainless steel stripe and a micropipette thermal sensor is described, the techniques for improving the durability and the reliability in data acquisition of micropipette sensor is justified, and the reliable method for determining the thermal conductivity of the micro scale SS 304 stripe and thin films of CNTs are explained. The micro scale SS 304 stripes (80µm × 6µm × 0.6µm) were fabricated using the focused ion beam (FIB) machining technology. The micropipette thermal sensors were fabricated using Seebeck effect principle and used to measure the temperature at different position on the surface of SS 304 stripe and thin films of CNTs. The durability and the reliability of the sensors were improved through rubber coating and bending of the sensor tip at the taper region in such a way that the pipette approaches and lands on the surface of the sample close to an angle of 90º. The rubber coating acts as a protective layer on the sensor tip while the ~90º bent pipette helps the erosion of the nickel coating at the tip by avoiding the skidding problem.

1.1 Objectives

The main objective of this research is to improve the reliability and the durability of the fabricated micropipette sensors, and to use them to characterize the thermal behavior of the SS 304 stripe at micro level, and of the CNT films of different thickness

at room temperature. Following are the list of specific objectives that have been achieved in this thesis:

- Fabrication and calibration of the micropipette thermal sensor
- Improvement in the durability and the reliability of micro-pipette thermal sensor
- Comparative study in the sensitivity of micropipette sensors before and after rubber coating
- Fabrication of the micro SS 304 Stripe (80µm × 6µm × 0.6µm)
- Measurement of the thermal conductivity of fabricated micro SS 304 stripe and comparison to other measured values and the simulated result
- Measurement of the thermal conductivity of thin films of CNTs of different thickness and characterization based on the film thickness

1.2 Organization of Thesis

The thesis has been divided into seven different chapters. A brief overview of the following chapters is summarized below:

Chapter 2 provides the information on the basic science that has been applied in this research study. It explains the way in which the heat-transfer principles and thermocouple principle was applied in the study. It elaborates the heat transfer theory from the perspective in which it has been implemented in the research. It also gives the information on the thermocouple circuit used while taking the reading from the pipette sensors.

Chapter 3 presents the literature review carried out throughout the research. Different methods carried out by the researches to measure the thermal conductivity have been described.

Chapter 4 gives the detail information on the methods and materials used to fabricate the SS 304 stripe and micropipette thermal sensors.

Chapter 5 focuses on the experimental setup used to carry out the experiment and the measurement techniques used to measure different parameters required to calculate the thermal conductivity value.

Chapter 6 summarizes the result obtained for the calibration of the micropipette thermal sensors, reliability test performed on the sensor, experimental and simulated result obtained for the SS 304 stripe, and the experimental result and comparison of different CNT films of varying thickness.

Chapter 7 gives the conclusion for all the work carried out for the thesis and possible future works that can be continued.

1.3 Works Cited

1. Shrestha, Ramesh. *High-presicion Micropipette Thermal Sensor for Measurement of Thermal Conductivity of Carbon Nanotubes thin film*. Master's Thesis. Denton: Univeristy of North Texas, 2011. Print.
2. Wu, C C and F B Wu. "Microstructure and Mechanical Properties of Magnetron Co-sputtered Ni-Al coatings." *Surface and Coatings Technology* (n.d.): 204. 854-859.
3. *Damascus Fortune*. 7 January 2013.
4. Ajayan, Pulickel M and Otto Z Zhou. "Applications of Carbon Nanotubes." n.d. *Rice University.* Document. 7 January 2013.
5. Bekyarova, E., et al. *J. Phys. Chem B.* (2004): 108.

6. Snow, E. S., et al. "Chemical Detection with Single-walled Carbon Nanotube Capacitor." *Science* (2005): 307.
7. Wu, Z., et al. *Science* (2004): 305, 1273-1276.
8. Artukovic, E., et al. *Nano Lett.* (2005): 5, 757-760.
9. Zhang, M., et al. *Science* (2005): 309, 1215-1219.
10. Zhang, D., et al. *Nano Lett.* (2006): 6, 1880-1886.
11. Gruner, G. *J. Mater. Chem.* (2006): 16, 3533-3539.
12. Yu, A., et al. *Appl. Phys. Lett.* (2006): 89.

CHAPTER 2

THEORITCAL BACKGROUND

This chapter covers the fundamental theories of science that has been applied in this research study. The chapter starts with the overview of heat transfer mechanism and the way they have been considered from the research point of view. Later part of the chapter focuses on the thermocouple principle based on which the micropipette sensors are fabricated.

2.1 Heat Transfer

Heat transfer is the energy interaction driven by the temperature difference between the system and its environment [1]. It is the energy in transit which is a result of temperature gradient. Thus, the temperature gradient is the driving force that causes heat to flow. It basically applies to a study where the primary concern is the mechanisms of energy transfer in the form of heat [2]. In thermal arts and sciences, they generally deal with four basic thermal transport modes: conduction, convection, phase change, and radiation [3]. Transfer of heat through a solid medium or a stationary fluid is the heat transfer through conduction. The transfer of heat due to bulk movement of a fluid over a wetted surface is termed as convection. Phase change is the term given when the fluid changes its state from liquid to solid or liquid to vapor. The energy transfer by defined range of wavelengths, 100nm to 1000μm [4], of electromagnetic radiation is the radiation mechanism of heat transfer. The detail explanation of the heat transfer mechanism involved in this research is explained below in detail.

2.1.1 Conduction

If the medium is not at thermal equilibrium, there occurs the heat transfer as a result of conduction and this heat transfer through conduction is governed by Fourier's law which states that the heat flux (heat transfer rate per unit area), q'', is proportional to the temperature gradient, ∇T, [4] i.e.,

$$q'' = -k.\nabla T \qquad (2.1)$$

where the proportionality constant,k, is the thermal conductivity and depends on the material property which may depend on temperature.

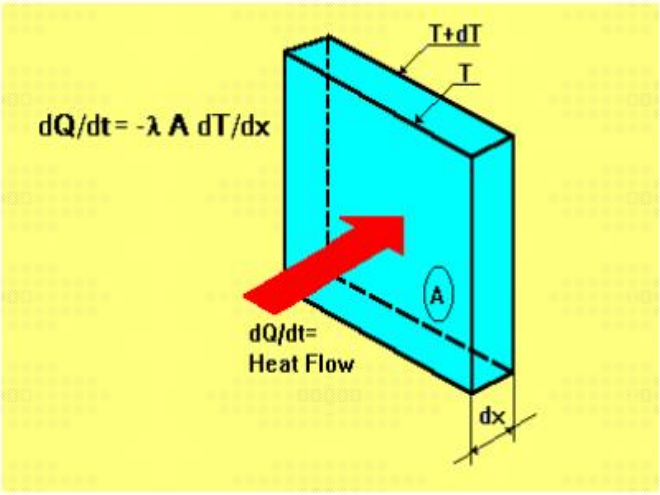

Figure 2.1: Schematic diagram showing one dimensional heat flow

For one-dimensional heat diffusion through solids with temperature varying only in x direction, the Fourier's law gives the heat flow as:

$$\dot{Q} = -k\,A\frac{dT}{dx} \qquad (2.2)$$

Where, $\dot{Q}$ = heat flow [W]

k = thermal conductivity [W/m°C]

A = surface area perpendicular to heat flow [m^2]

$\frac{dT}{dx}$ = temperature gradient along x direction [°C/m]

Similarly, for cylindrical coordinate system the heat diffusion through solids with temperature varying only in radial direction, the Fourier's law gives the heat flow as:

$$\dot{Q} = -k\,A\,\frac{dT}{dr} \qquad (2.3)$$

Where, $\dot{Q}$ = heat flow [W]

k = thermal conductivity [W/m°C]

A = surface area perpendicular to heat flow [m^2]

$\frac{dT}{dr}$ = radial temperature gradient [°C/m]

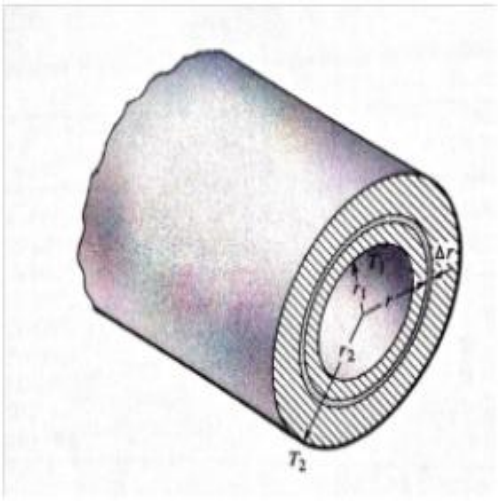

Figure 2.2: Schematic diagram showing heat flow in radial direction

2.1.2 Convection:

Convection is the heat transfer mechanism which involves the transfer of thermal energy due to the flow of fluids or gases from one place to another. It is the mechanism of heat transfer which is in between a surface and a moving fluid at different

temperatures [5]. They play a dominant role in the heat transfer mechanism in liquids and gases. Based on the mechanism convection can be classified into two categories: forced and natural. In the experiment I am concerned about the natural convection phenomena which might contribute to the heat loss from the surface of the sample.

2.1.2.1 Natural Convection

Natural convection, also referred to as a free convection, is caused by buoyancy force as a result of difference in density caused by temperature variations in the fluid. When the body is heated there is the change in the density of the fluids surrounding the boundary layer of the body. This change in density of the fluid causes it to rise and be replaced by high density fluid or cooler fluid which in turn gets heated and rise [5]. This process, which continues till the stable state is attained, is called natural convection.

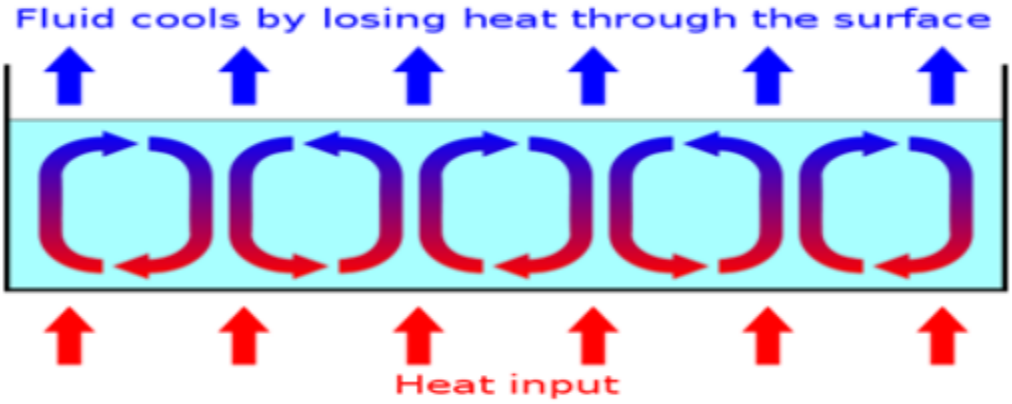

Figure 2.3: Schematic diagram showing convectional heat flow

In order to analyze all the heat loss from the sample during the experiment there is a need to take natural convection phenomena into consideration which might significantly affect the thermal conductivity measurement. From Newton's law of cooling, the heat transfer per unit surface through convection is given as:

$$\dot{Q} = h\,A\,(T_s - T_f) \qquad (2.4)$$

where: h= convective heat transfer coefficient [W/m^{2}K]

A= surface area [m^2]

T_f = averaged fluid temperature [K]

T_s = surface temperature of sample [K]

In natural convection, the motion of fluid is due to difference in the densities of the fluids. These fluids are subject to be acted on by the local gravitational and centrifugal forces. The magnitude of these forces determines the convective heat transfer coefficient in equation 2.4. The velocity and the local gravitational and centrifugal forces have the direct relation, so, the velocities are usually small for cases where the local gravitational and centrifugal forces are small [6]. Under these circumstances, Grashof and Rayleigh number determines the fluid flow behavior instead of Reynolds number. According to Churchill and Chu [7] the flow for the horizontal heated cylinder is laminar if the Rayleigh number is within a range of 10^{-6} and 10^{9}. The expression for Rayleigh number and Grashof number is given as:

Rayleigh number $$\mathrm{Ra_x} = \mathrm{Gr_x}\,\mathrm{Pr} \tag{2.5}$$

where, $\mathrm{Gr_x}$ = Grashof number

Pr= Prandtl number

Grashof number $$\mathrm{Gr_x} = \frac{\beta\,\Delta T\, g\, x^3}{\nu^2} \tag{2.6}$$

where, β= volumetric coefficient of expansion [1/K]

g= acceleration due to gravity [m/s^2]

ΔT= temp. difference between surface and fluid[K]

x = characteristic length [m]

α = thermal diffusivity [m^2/s]

v= kinematic viscosity [m^2/s]

The Nusselt number for any arbitrary shaped object with laminar natural convection boundary layer condition is defined by Lienhard [7] as:

$$\overline{\mathrm{Nu_x}} = 0.52\ \mathrm{Ra_x^{1/4}} \tag{2.7}$$

where: x = characteristic length [m]

D = diameter of cylinder [m]

The expression for Nusselt number, equation 2.8, determines the average heat transfer coefficient which in turn will determine the heat loss as a result of natural convection from Newton's law of cooling. The expression for Nusselt number is given as:

$$\overline{Nu_x} = \frac{\overline{h_x} D}{k} \tag{2.8}$$

where, $\overline{h_x}$ = avg. heat transfer coefficient [W/m^{2}K]

D = diameter of cylinder [m]

Thus, the heat loss due to natural convection can be calculated.

2.1.3 Radiation

Radiation is simply defined as the electromagnetic waves travelling in the space. These electromagnetic waves carry energy. When they come in contact with an object the energy of these waves gets transferred to an object in the form of heat. All matter which has a temperature greater than the absolute zero emits thermal radiation as they have atoms or molecules with the changing kinetic energy. This kinetic energy result in the dipole oscillation of charges or/and charge acceleration, and these motions of charges emit electromagnetic radiation waves. The net energy radiated by the hot object to its cooler surrounding environment is given by Stefan-Boltzmann law as

$$P = e\sigma A(T^4 - T_c^4) \tag{2.9}$$

Where P = energy radiated [W]

e = emissivity of an object

σ = Stefan-Boltzmann constant [5.6703 × 10^{-8} W/m^2K^2]

A = area [m^2]

T = temperature of hot object [°C]

T_c = temperature of the surrounding [°C]

In this research I use laser radiation as a source of energy to heat the sample.

2.2 Thermocouple Principle

Seebeck (1770-1831) discovered that when two different conductors “metal 1” and “metal 2” are connected together at the hot point and a temperature difference (dT) is maintained between this point and the cold point (figure 2.4), then an open circuit voltage (dV) is developed between the two conductor wires at the cold point [8]. This effect is known as Seebeck effect.

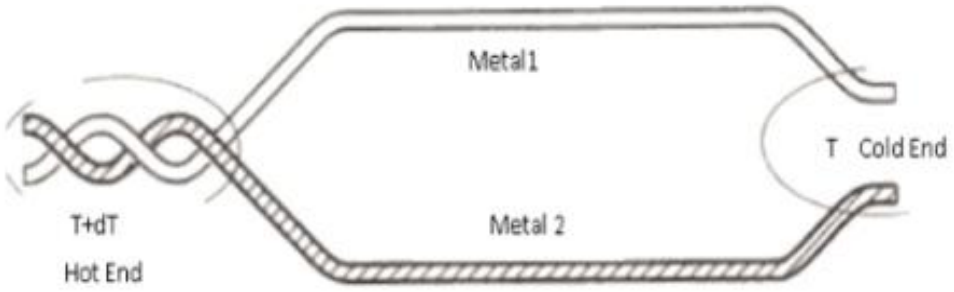

Figure 2.4: Schematic diagram reflecting Seebeck effect

The physics behind the phenomena is that when a temperature gradient is introduced along the length of a metal wire, electrons start to diffuse from one end to the other end of the wire. The direction of electron diffusion depends on the electrical

properties of the metal wire. If the electron diffuses from the hot end towards the cool end of the wire then a negative thermoelectric electro motive force (emf) is generated in the wire with respect to the hot end (by convention) and vice-versa [2]. Only the combination of two different materials exhibits the Seebeck effect, and, thus, called the thermocouple. The Seebeck effect is not shown for a two metals of the same material because of the symmetry. Also, Seebeck effect is a bulk property and does not depend on a specific arrangement of the metals or the materials or the specific way of joining them [8].

Different metals have different thermoelectric sensitivities, or Seebeck coefficients. Seebeck coefficients are defined as the ratio of change in voltage with respect to a change in temperature. For example, Seebeck coefficient of gold is 6.5 μV/K; which implies that for every 1K temperature change, a positive thermoelectric emf (Seebeck voltage) of 6.5 is induced in gold at temperature around 0ºC. Seebeck coefficient may ether be positive or negative depending on the materials. The Seebeck voltage and temperature tends to show a linear relationship for the small change in temperature, whereas, for larger temperature ranges, the relationship is nonlinear, so, it is necessary to state the temperature at which the Seebeck coefficient is being specified [9].

Let the metals 1 and 2 are made up of two different materials joined at one end which has the Seebeck coefficient of S_1 and S_2 respectively. Let the emf or Seebeck voltage produced be "S_v" and the temperature difference between the hot and cold end be "dT" then the Seebeck effect can be mathematically expressed as

$$S_v = \frac{(S_1 - S_2)}{dT} \qquad (2.10)$$

where, $S_1 = S_2$ = Seebeck Coefficient expressed in V/K or uV/K

2.2.1 Thermocouple Circuit

The following figure 2.4 gives the schematic diagram of the thermocouple circuit used in the experiment. The metal subjected to a thermal gradient generates Seebeck voltage according to the Seebeck effect, in order to measure this voltage there is a need of voltmeter which has to be connected using another lead wire (copper wire in this research) from voltmeter. This additional lead wire will create its own Seebeck voltage when an extra junction is created. This voltage generated tends to oppose the original voltage whose magnitude depends on the Seebeck coefficient of the used metals.

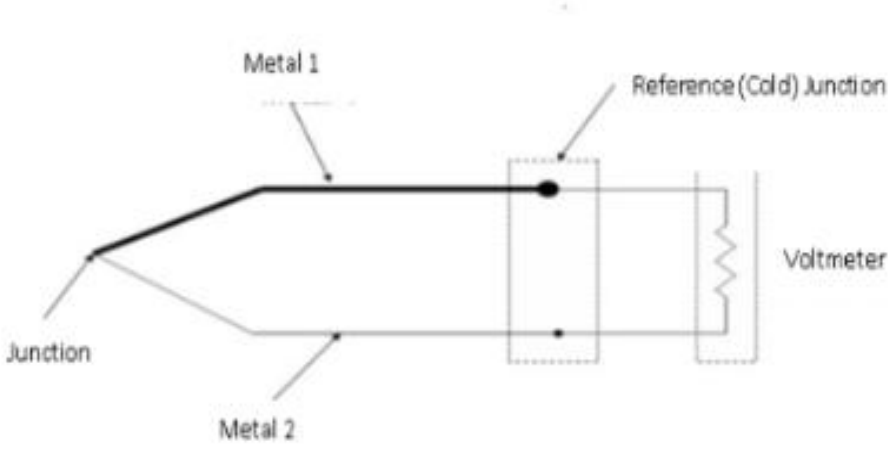

Figure 2.5: Thermocouple circuit used in the experiment

In the figure 2.5, metal 1 and metal 2 create a junction at tip which is used to sense the temperature of the surface of the sample when two of them come in contact. When the lead wires are connected to connect these wires to the voltmeter the reading displayed by the voltmeter is not the actual voltage reading, rather, it is the total cumulative voltage reading which is affected by the lead wires connecting metal 1 and

metal 2 at the reference junction. In order to neutralize the Seebeck effect at the reference junction there is a need of cold junction compensation.

2.2.2 Cold Junction Compensation

Thermocouple only gives the relative temperatures rather than the absolute temperature. So, in order to know the absolute temperature there is need of thermocouple circuit with a known reference temperature like ice bath. In order to be able to measure the absolute temperature the cold junction i.e. the reference junction should be maintained at the known reference temperature. This principle is known as cold junction compensation.

One way to do is to put the reference junction into the ice bath which is cumbersome and impractical in an ambient environment. There is an artificial cold junction commercially available which uses thermally sensitive devices like thermistor, diode or resistance thermometer to measure the temperature of the instrument at the input connections.

Cold junction compensation for this research is done by maintaining the reference junction at a constant temperature of 25°C based on the fact that the two junctions maintained at the same constant temperature has voltages generated in equal amount but in opposite directions. Thus, the net voltage due to an extra junction will be zero.

2.3 Works Cited

1. Bejan, Adrian. *Advanced Engineering Thermodynamics*. New Jersey: Wiley, 2006. Print.
2. Janna, Willam S. *Engineering Heat Transfer*. CRC Press, 2000.

3. Bejan, Adrian and Allan D. Kraus. *Heat Transfer Handbook*. New York: J. Wiley, 2003. Print.
4. Zhang, Zhuomin M. *Nano/microscale Heat Transfer*. McGraw-Hill, 2007. Print.
5. *Convetive Heat Transfer*. Website. 11 March 2013.
6. Burmeister, Louis C. *Convective Heat Transfer*. New York: Wiley, 1983.
7. Mills, A. F. "Heat and Mass Transfer." *California: Library of Congress Cataloging in Publication Data* (1995).
8. Van-Herwaarden, A. W. and P. M. Sarro. "Thermal Sensors Based on the Seebeck Effect." *Sensors and Actuators* (1986): 321-346. Print.
9. Molki, Arman. "Simple Demonstration of the Seebeck Effect." *Science Education Review* (2010): 103-107.

CHAPTER 3

LITERATURE REVIEW

There are different methods developed and implemented by scientists all around the world to measure the thermal conductivity of micro stripes and thin films. These methods are good for a particular research in which they are involved but are not competent enough to be used for other similar researches in which there is a change of few parameters. Thus, the particular method developed for particular research lacks the versatility to be used for other research purposes. The constraint being the fact that different class of stripes and thin films has different sets of characteristic properties. So, it is cumbersome to characterize all class of stripes and thin films with one particular method and experiment set up, rather there is a need of some modification and even new experiment set up to overcome the obstacle for each particular case of stripe and thin films. In spite of all the problems faced, there are methods which have been successfully developed and implemented to thermally characterize stripes and thin films. Some of method discovered through the literature research is discussed below in detail.

This chapter gives the information on different measuring techniques employed for the thermal characterization of the materials. A brief summary of the steady state, quasi steady state, transient, microprobe, and bolometric technique for measuring the thermal transport property of the materials is presented in this chapter. In general, steady state method is used for measuring thermal conductivity and transient method is used for measuring thermal diffusivity [1]. Since, the research is based on the steady

state technique different steady state techniques for measuring the thermal conductivity has been discussed with prime concern.

3.1 Steady State Method

Steady-state methods are generally used for the measurement of the thermal conductivity [1]. Steady-state techniques are based on the Fourier's law of heat conduction and are useful for the experiment where the temperature of the material is independent of time i.e. temperature does not change with time. As the temperature remains constant with the time, the constant signal is obtained during the experiment which makes the data analysis straightforward. The only drawback with this method is that there is a need of well-engineered experimental setup. It also consumes a lot of time compared to other methods as the experiment takes time to settle at the constant steady state temperature during the experiment. According to Hammerschmidt [2], the thermal characterization for a steady state measurement at a one dimensional temperature field can be done by at least two thermometers at two different fixed positions. Based on the similar concept I used one micropipette sensor at two different positions to thermally characterize the sample. Some of the steady state method that has been successfully applied for measuring the thermal conductivity of the materials is explained below.

3.1.1 Guarded Hot Plate Method

As the name implies guarded hot plate method consists of a hot plate placed at the center while the whole setup is being isothermally guarded with the isothermal cold plates. This method works on the principle of steady state and can be used to thermally characterize solid, composites, homogeneous, insulation and opaque materials. The

schematic diagram is given below in figure 3.1.This method uses two samples of identical shape and size with a known sample thickness and the area to thermally characterize the sample. Both the samples used can be the real sample whose thermal conductivity is to be determined or just a sample by itself and a dummy sample. The two

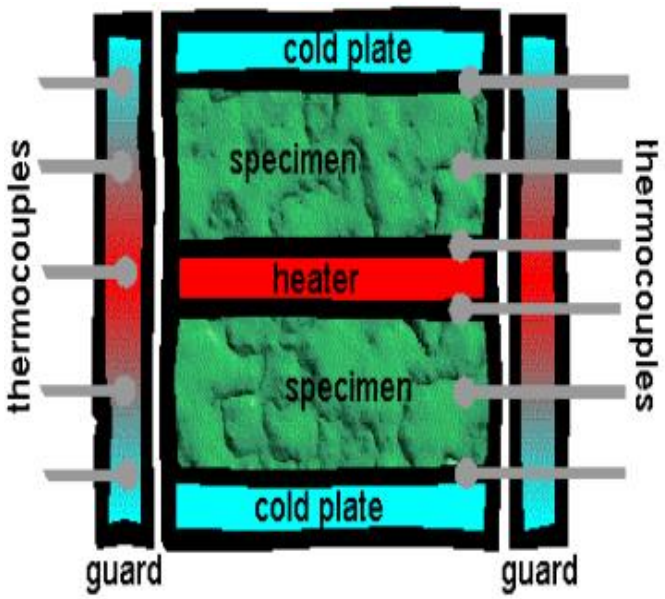

Figure 3.1: Schematic diagram of guarded hot plat method [3]

samples are not in touch with each other and are separated by the guarded central hot plate placed in between them. They are isolated from the external environment by the isothermal cold plates. Both the guarded central hot plate and the isothermal cold plates are fully controllable. The surface of the cold plates are blackened so as have a high emittance. The temperature at different position is measured with thermocouples embedded at different positions in between two cold plates [3].

During the experiment a known direct current (DC) power is applied to the hot plate while the temperatures in cold plate and guard sections are adjusted to maintain the two different uniform temperatures over the surface of two samples. After the establishment of thermal equilibrium the power and the temperature differences in

between two samples are recorded such that the average thermal conductivity is calculated for the total sample area and thickness. This is the way to determine the thermal conductivity value when two samples are used. In the case when a sample and a dummy sample are used for the experiment the temperature for the dummy sample is sought at zero and the thermal conductivity is directly calculated for the sample [3].

The working principle for this method is simple but there are certain circumstances before it can actually be used to measure the thermal conductivity value. In order to use this method the sample used in the experiment should be flat and parallel within the limits of ISO Standard 8302. The thickness of the sample must represent that of bulk material. The thickness also determines the plate size which must be greater than ten times the dimension of the largest constituent material. In order to measure the thermal conductivity of hard materials and the materials with higher thermal conductivity value the thermocouple must be separately instrumented in order to minimize the contact resistances between surfaces [3].

3.1.2 Heat Flow Meter Method

The basic operating principle of the heat flow meter method is similar to that of the guarded hot plate method. The only difference is the way the heat flow is determined through the sample. The heat flow meter uses the heat flux sensors which are permanently installed and calibrated within the apparatus [4]. A schematic diagram is shown in figure 3.2. A thermally insulated sample is sandwiched and guarded from the external environment in between the hot and cold plates which are maintained at different constant temperatures. During the experiment the sample is allowed to settle to equilibrium [4].

Like every other methods this method also has certain requirement and limitations. Similar to the guarded hot plate method the sample should meet the size and thickness requirement to be able to implement this method. The sample must be flat and parallel within the limits of ISO Standard 8301. This method is not suited for hard materials and materials whose thermal conductivity value is less than 0.3 W/(m.K). The plate temperature should be controlled within ±0.1 K. The stability and reproducibility of heat flux transducer, which are made from highly stable material, over the temperature range of continuous operation is of critical factor [4].

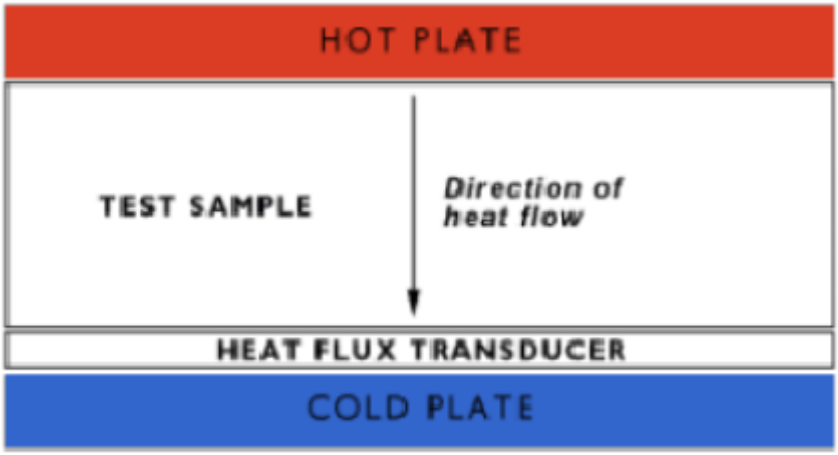

Figure 3.2: Schematic diagram of heat flow meter method

3.1.3 Radial Heat Flow Method

Radial heat flow method is based on the principle of the Fourier's law of heat conduction for a cylindrical body. A cylindrical heat source is placed at the center of the cylindrical sample whose diameter is indefinitely larger than that of the central heat source [5]. The sample is guarded by the heaters placed at the two ends, and chosen in such a way that the ratio of length to diameter of the sample is relatively large to avoid the end effects.

During the experiment the sample is centrally heated at constant power till the steady state is established. The temperatures at two different radial positions are then measured with the help of the temperature sensors located inside the sample. With the known value of heating power, temperatures at two different radial positions, and the length of cylindrical sample the thermal conductivity is determined using the Fourier's equation for the heat conduction in radial direction

$$\dot{Q} = -\frac{2\pi k L (T_1 - T_2)}{\ln(r_2 / r_1)} \qquad (3.1)$$

Where, T_1, T_2 = temperature at two radial position [°C]

L = length of cylinder [m]

r_1, r_2 = radial positions [m]

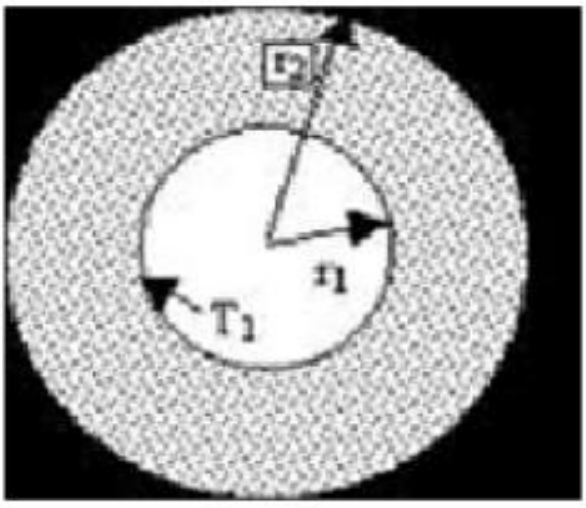

Figure 3.3: Radial heat flow method positioning

3.2 Transient Method

Transient methods are based on the rate of change of temperature and include thermal wave technique and pulse technique, frequency domain and time domain respectively. They are generally used for the measurement of the thermal diffusivity [1],

but are popular among the researches to measure the thermal conductivity because it doesn't require precise alignment, dimension knowledge and stability [6]. Moreover, the speed of measurement is faster compared to that of steady state method. The reliability of the results acquired from this method strongly depends on the initial and final boundary conditions of the experiment as the certain minor change in the experimental environment would result in different sets of data. So, an extra care and observation is required. In order to characterize the time dependent temperature within a known position of a sample, one thermometer would be enough [2]. Different transient strip methods have been implemented for thermal characterization of materials. A brief summary of the transient hot strip method developed by Gustafsson et al. is given below.

3.2.1 Transient Hot Strip Method

Gustafsson et al. [7] had developed transient hot strip method for simultaneously measuring thermal conductivity and thermal diffusivity of solids and fluids. The method is based on recording the rise of temperature of the plane metal strip surrounded by material whose thermal properties are to be measured. The plane metal strip is sandwiched between the material slabs during the study of the solid materials, whereas, suspended vertically during the study of the fluids. It is used both as a constant source of heat and a temperature sensor.

During the experiment a constant direct current is supplied to the plane metal strip such that the output power stays constant. Over a short period of time the voltage drop over the strip is recorded as a function of time. There is a change in the recorded voltage which is due to the rise in the temperature, as the rise in temperature tends to

increase the electrical resistance of the metal strip. With this voltage drop over the strip and the temperature coefficient of the strip resistance the rise in the temperature of the strip is calculated. The temperature rise is then used to characterize the materials surrounding the plane metal strip. This is an absolute method and the thermal conductivity of the material is calculated from the temperature of strip as a function of time, the dimension of strip, the current and the voltage drop [7].

The cross section geometry of the heating element is of very important as the time scale for measurement is limited, which means that there is an appreciable increase in the temperature only in the immediate neighborhood of the heating element. For a particular investigation the cross section of the plane metal strip used was approximately 4mm × 0.008mm i.e. the thickness to the breadth ratio of the strip is 0.002 [7]. Also, in order to minimize the effects of finite strip length the ratio of strip length to width had to be kept larger than 20-30 [8].

To measure the thermal conductivity of materials with higher values the size seems to be the limiting factor as the strip length to width ratio had to be kept larger than 20-30 to minimize the effect of finite strip, and the width of the strip (hence the length of the strip) is inversely proportional to the thermal conductivity of the materials. Another aspect that needs to be considered is the fraction of the heat that is withheld by the air or oil filled slots created at the edges of the strip when pressing the strip in between the materials whose thermal properties are being studied [7].

3.3 Quasi Steady State Method

Quasi steady state method is based on both the steady state and the transient technique. It uses the temperature that is changing with the time, either varying linearly

with the logarithm of time or time scale itself, for the mathematical analysis of the experiment. The analysis is done for the transient heat equation based on a quasi steady state solution over a long period of time [9].

> The ideal quasi-steady state mode works with a resistive heat source that is entirely embedded inside the specimen without any thermal contact resistance. The electrical input power is totally converted into a rate of heat flow that is liberated immediately and exclusively to the finite (!) specimen. The specimen is free to lose heat to the surroundings as long as boundary conditions vary with time only. The temperature field of the specimen may be far from thermal equilibrium; the field's profile should be cylindrical. Thus, a line- or strip-shaped source is considered in an arrangement that is most similar to the know THW or THS setup. [2]

A quasi steady state mode to the transient hot wire and the transient hot-strip techniques, introduced for the first time by Hammerschmidt, is based on both the steady state and transient techniques. This technique avoids the major drawbacks of both the steady state and transient techniques and utilizes the only characteristic properties of both the techniques. With an addition of a temperature sensor to the transient hot strip arrangement a differential signal is generated. This signal gives the time invariant measure of the thermal conductivity of the sample material under test. The homogeneous isothermal, convective and adiabatic boundary conditions allows signal to settle without being affected. The instrument, thus, operates under quasi steady state conditions which links the transient and the steady state technique together during the experiment after the transients die out. Here the temperature can be measured within a center region of the heat source which eliminates the need of guard heaters as the outer boundaries are free to change with time.

3.4 Microprobe Technique

The microprobe technique developed by Zhang et al. [10] demonstrates the capability to measure both thermal conductivity and the Seebeck coefficient simultaneously by utilizing the concept of thermoelectric energy conversion efficiency. Their thermo electric probing technique is based on an analytical heat transport model which can quantitatively elaborate the tip sample heat transfer. The microprobe has a willaston wire (5 micron diameter Pt-Rh core cladded with a 75 micron diameter silver shell) bent to “V” shape. The central part of the “V” shape is etched over a length of 200 micron to expose Pt-Rh core. The microprobe serves as a heater, thermometer and voltage electrode. It is heated using an alternative current (AC) whereas the direct current (DC) from the electrical power generates DC temperature rise. This temperature is greater than the ambient temperature in the sample and a DC Seebeck voltage across the sample. When the microprobe is in contact with the surface of the sample the probe temperature increases with the increasing input electrical power showing a linear relation. The slope given by the linear relation gives the effective thermal resistance of the probe. The rise in the temperature of the probe wire, which is averaged along its length, is determined from the measured value of electrical resistance of the probe and the calibrated temperature coefficient of resistance. This thermal resistance of the microprobe gives the measurement for the thermal conductivity [10].

In this technique microprobe has a different uses. It is used as a heater, thermometer and voltage electrode which reduces the number of equipment and the control of the experiment can be done easily. But the fact that the opening at the tip

which is primarily responsible for heat transfer is an issue with this measuring technique. The thermal characterization is best done with the smallest tip size as it will be more sensitive and omits the heat loss. In my research I have noticed the difference in the data acquisition using different tip sizes. By reducing the tip size of the sensor from 2µm to 1µm I was able to reduce the error in measurement by half.

3.5 Bolometric Technique

Bolometric technique utilizes the infrared radiation as a source of heat and the single-walled carbon nanotube (SWNT) film as resistive thermometer to measure the thermal conductivity of ultrathin films of SWNTs. The method developed by Itkis et al. [11] generates a triangular temperature profile along the suspended SWNT film for its thermal characterization. The technique studies the thermal conductivity of an as-prepared (AP) SWNT film obtained in the electric arc discharge process and a film of purified SWNTs prepared by vacuum filtration [11].

The bolometric configuration consists of a narrow ribbon of semitransparent SWNT film suspended across the opening in a sapphire ring. The silver paste, which is an efficient heat sink, was used to make an electrical contact to the SWNT sample. The length of SWNT sample was 3.5-4.0mm. The heat was supplied by the radiating an infrared light. The absorbed heat propagates from the center towards the electrical contacts without loss thereby generating a triangular temperature profile with maximum temperature in the middle and average temperature increment [11]. The thermal conductivity of the film is determined by

$$K = \frac{\mathrm{P_{abs}}}{\mathrm{dT}} * \frac{L}{8A} \qquad (3.2)$$

Where, P_{abs} = absorbed power of infrared radiation

A= cross sectional area of the SWNT film

dT = temperature difference

L= length of the sample

This method has the similar calculation procedure as I have used for the calculation except for the average temperature increase which is half the maximum temperature increase in this method. Instead of measuring temperature on the surface of SWNT this method uses electrical contacts on the boundary and averages out at the center which might be an issue.

Table 3.1 gives the information of different types of measurement method based on the type of material, the temperature range and the property range of the materials within which the method can be implemented.

Table 3.1: Measurement methods based on material type, temperature and property [1]

Measurement Method	**Material Type**	**Temperature Range(°C)**	**Property Range (W/(m.K))**
Comparative Technique	All Solids	0 – 1000	0.2 – 200
Four-Probe Technique	Metals and Metallic Alloys	20 – 1600	10 – 800
Guarded Heat Flow Method	Rocks, Polymers, Ceramics, Foods, Few Metals and Alloys	100 – 300	0.2 – 20
Guarded Hot-Plate	Solid, Opaque, Insulation Materials, Composite	-180 – 1000	0.0001 – 2
Heat Flow Meter Method	Insulation Materials	-100 – 200	0.007 – 1.0
Hot-Box Apparatus	Wood, Glass, Masonry, system with insulation and other products used in the building	-20 – 40	Thermal Conductance of 0.2 – 5 (m^2K)/W
Hot Stripe Method	Ceramics, Foods, Glasses etc.	-50 – 500	0.1 – 5

3.6 Works Cited

1. "Measurement Methods." *evitherm (Virtual Institute for Thermal Metrology).* Website. 11 March 2013.
2. Hammerschmidt, U. "A Quasi-Steady State Technique to Measure the Thermal Conducitivity." *International Journal of Thermophysics* (2003). Print.
3. "Guarded-hot-plate Method." n.d. *evitherm (Virtual Institute for Thermal Metrology).* Website. 11 March 2013.
4. "Heat-flow meter method." n.d. *evitherm (Virtual Institute for Thermal Metrology).* Website. 11 March 2013.
5. Mills, A. F. "Heat and Mass Transfer." *California: Library of Congress Cataloging in Publication Data* (1995).
6. Assael, Marc J. and William A. Wakeham. "Thermal Conductivity Measurment." *Mechanical Variables Measurment: Solid, Fluid and Thermal*. 14-1-4-9. Print.
7. Gustafsson, S. E., E. Karawacki and M. N. Kahn. *J. Phys. D* (1979): 1411.
8. Gustafsson, S. E., E. Karawacki and M. A. Chohan. *J. Phys. D* (1986): 727.
9. Ho, Kai and Robert D. Pehlke. "Simultaneous Determination of Thermal Conductivity and Specific Heat for Refractory Materials." *Journal of American Ceramic Society* (1990): 316-322. Print.
10. Zhang, Yanliang, et al. "A Micrope Technique for Simultaneously Measuring Thermal Conductivity and Seebeck Coefficient of Thin Films." *Applied Physics Letters* (2010): doi: 10.1063/1.3300826. Print.

11. Itkis, Mikhail E., et al. "Thermal Conductivity Measurements of Semitransparent Single-Walled Carbon Nanotube Films by a Bolometric Technique." *Nano Letters* (2007): 900- 904. Print.

CHAPTER 4

METHODOLOGY AND MATERIALS

The chapter covers the methods and materials used in the research. It gives the detail information on the machining tools used in order to furnish the final product used for the experiments.

4.1 Fabrication of the Stainless Steel 304 (SS 304) Stripe

A micro scale stainless stripe was fabricated from a piece of stainless steel sheet in two different steps. The procedures followed and the machines used for the fabrication of the stripes are discussed below.

4.1.1 Sample Etching and Polishing

Etching is the process of chemical corrosion of the material surface conducted in a controlled manner to reveal microstructure details. The material undergoes volumetric reduction during the etching process. I applied the etching solution to the raw stainless steel to reduce its volume. The reduced stainless steel was then polished using ultra fine abrasive to smoothen and brighten the surface for FIB machining.

4.1.2 Machining

For the preparation of the sample I used the dual beam FIB/ FSEM Nova 200. As the name implies it has a dual beam platform comprising of focused ion beam (FIB) and scanning electron microscope (SEM) for imaging, material removal, and deposition at length scales ranging from few nanometers to hundreds of microns. It is a powerful tool used for nanomanipulation and fabrication through the augmentation of FIB instrument with micromanipulation and gas injection from local chemical vapor deposition (CVD)

[1]. These tools are used in material characterization, industrial failure analysis and process control application which is sought as the preferred solution for 3D microscopy and analysis. They are designed to deliver integrated sample preparation and microanalysis below 1nm for high throughput semiconductor and data storage fabs and materials science and life science labs [2].

4.1.2.1 Scanning Electron Microscope (SEM)

Scanning electron microscope is a type of electron microscope which uses concentrated focused beam of high energy electrons to scan the sample and produce images of those samples. These high energy electrons incidents on the surface of the sample and generate different signals at the surface of the sample. These signals from electron sample interaction can be detected which reveals information about the sample's surface topography, composition, crystalline structure and orientation of materials making up the sample. The electron beams are generally scanned in a raster scan pattern, and the intensity of the secondary electrons produced at each raster position of the beam is displayed to create an image of the sample [3].

Based on the need and circumstances the areas ranging from 1cm to 5µm (approximately) in width can be imaged in scanning mode using conventional SEM techniques whose magnifications ranges from 20X to 30,000X (approximately) and spatial resolution of 50nm to 100nm [4]. The SEM can also perform analyses of selected point locations on the sample. It can qualitatively or semi-quantitatively determines chemical compositions using EDS, and determine crystalline structure, and crystal orientations using EBSD.

During the operation, the electrons with significant amount of kinetic energy are accelerated towards the sample under study. After the interaction with the sample it gets decelerated and loses its energy which is used to produce variety of signals. The produced signal includes secondary electrons, backscattered electrons, diffracted backscattered electrons, photons, visible light, and heat. For the purpose of imaging, the secondary and backscattered electrons are commonly used. Secondary electrons are important for showing morphology and topography on samples, whereas, backscattered electrons are important for illustrating contrasts in composition in multiphase samples. Unlike FIB, SEM analysis is considered to be non destructive method as x-rays generated by electrons interactions do not lead to volume loss of the sample and the same sample can be used again and again for analysis [4].

4.1.2.2 Focused Ion Beam (FIB)

FIB microscope is a versatile tool which enables inspection, characterization, structuring or manipulation for a broad range of materials. It has both imaging and micromachining capabilities at the nanometer-micrometer scale [1]. It looks and operates similar to SEM. It consists of a vacuum system and chamber, a liquid metal ion source, an ion column, a sample stage, detectors, gas delivery system, and a computer to run the complete instrument [3]. The main difference between FIB and SEM is the use of different particle to create the primary beam that interacts with the sample. Here, FIB uses ions whereas SEM uses electrons. Moreover, FIBs can scan over the surface of the sample to create an image and can be controlled to locally expose the sample to the beam by a patterning function. Similar to the SEM imaging principle, the ion beam in FIB is directed towards the sample which after reacting with the sample generates

signals or secondary ions. The detected secondary ions are used for the imaging which has magnifications up to ~100,000X with very good depth of field [3]. The focused ions are huge compared to electrons because of which they sputter away atoms from the surface of the sample after interaction. Moreover, the gas chemistry can be injected close to the surface of the sample and allow material deposition or material dependent selective etching [5].

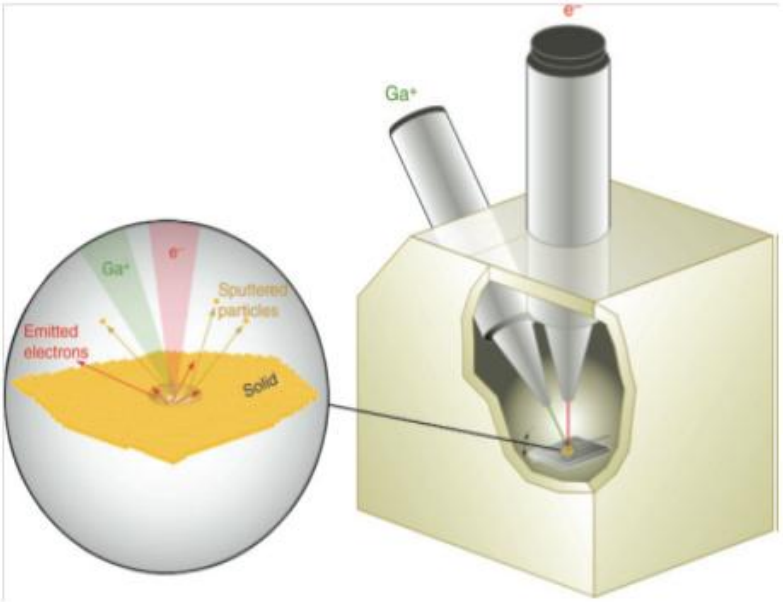

Figure 4.1: Schematic diagram of dual beam FIB/FSEM [1]

A liquid metal ion source is the base of focused ion beam system which can be focused into diameters smaller than 10nm with current densities of several A/cm^2. FIB can be used for programmed fabrication of features on a sample on a sub-micrometer scale by removing the material from the sample by sputtering (micromachining) and for the addition of materials to the sample by ion induced reactions at sub-micron dimensions (deposition) [6]. FIBs are basically used for failure analysis, characterizing defects, modifying design etc.

FIB operation begins with a liquid metal ion source (Gallium ion). Gallium (Ga) has low melting point which enables it to exist in the liquid state near room temperature, and it can be focused to a very fine probe size (10nm in diameter). A Ga reservoir is positioned in contact with a sharp tungsten needle. The Ga wets the tungsten needle and flows to its tip. This fine tungsten tip is now used as an ion source from which Ga atoms are extracted and ionized via high tensions. As a result of high extraction field (>10^8 V/cm) the liquid Ga is pulled into a sharp cone whose radius ranges from 5nm to 10nm [3]. As a result of field ionization and post ionization, ions are emitted and accelerated down the FIB column. FIBs generally operate within the range of 5keV to 50keV accelerating voltage which accelerates Ga+ ions and focuses on the sample through the electrostatic lenses [7]. By controlling the strength of the electrostatic lenses and adjusting the effective aperture sizes, the probe current density (and therefore beam diameter) may be altered from tens of pA to several nA corresponding to a beam diameter of ~5nm to ~0.5µm [3]. The impacting ions can interact with the sample material in many different ways, such as the emission of electrons, ions, atoms or clusters. To use those emitted particles different detectors are attached which generate images with different information [7].

The piece of SS 304 was reduced to the thickness of ~600 nm after the etching and polishing of the raw SS 304.The polished SS 304 was then subjected to the FIB machining. In the FIB, a desired shape and dimension of the sample was patterned and milled (80µm × 6µm). The milled sample was then lifted up and placed on the chip with the help of omniprobe (nanomanipulator). The sample was glued to the chip with the

help of platinum using gas injection system (GIS) needle. The systematic drawing for the whole process is shown below:

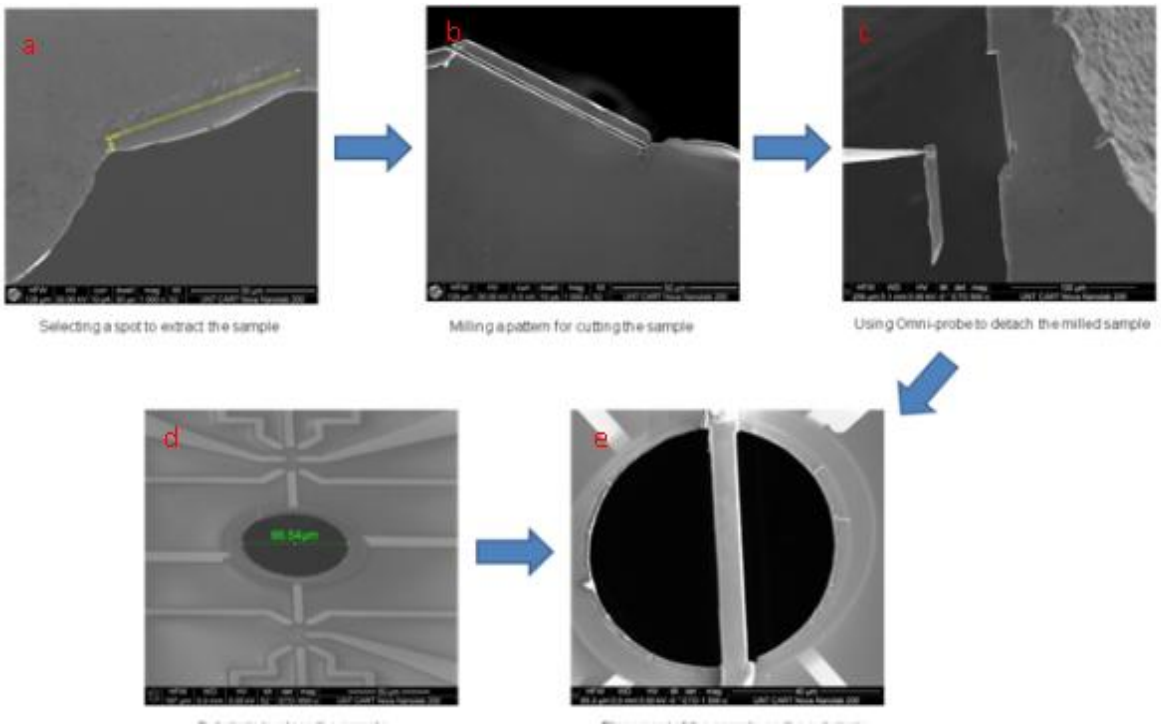

Figure 4.2: Fabrication of stainless steel stripe: (a) selecting a spot to extract the sample; (b) milling a pattern for cutting the sample; (c) using omni-probe to detach the milled sample; (4) substrate to place the sample; (e) placement of the sample on the substrate

4.2 Fabrication of Micropipette Sensors

In order to characterize the thermal property of the materials I used the micropipette thermal sensors based on the thermocouple principle. The two different materials that was used to fabricate the sensors are Nickel (Ni) and the solder alloy (alloy of Tin (Sn)). A thermocouple junction was created at the tip of the micro pipette whose diameter is controlled around ~1µm. The following basic methods were undertaken during the fabrication of fully functional micro pipette thermal sensors:

4.2.1 Fabrication of the Pipette from a Borosilicate Glass

This is an initial step during which a micrometer sized pipette is fabricated from a thick walled borosilicate glass tube which has an outer diameter (OD) of 2mm and the inner diameter (ID) of 1.56mm. A pipette puller (P-97, Sutter Instrument) is used to pull the pipette from a glass tube. Based on the need and circumstances the pipette puller was programmed making sure that the tip size of the pipette was ~1µm and taper length of 5mm to 7mm (approximately).

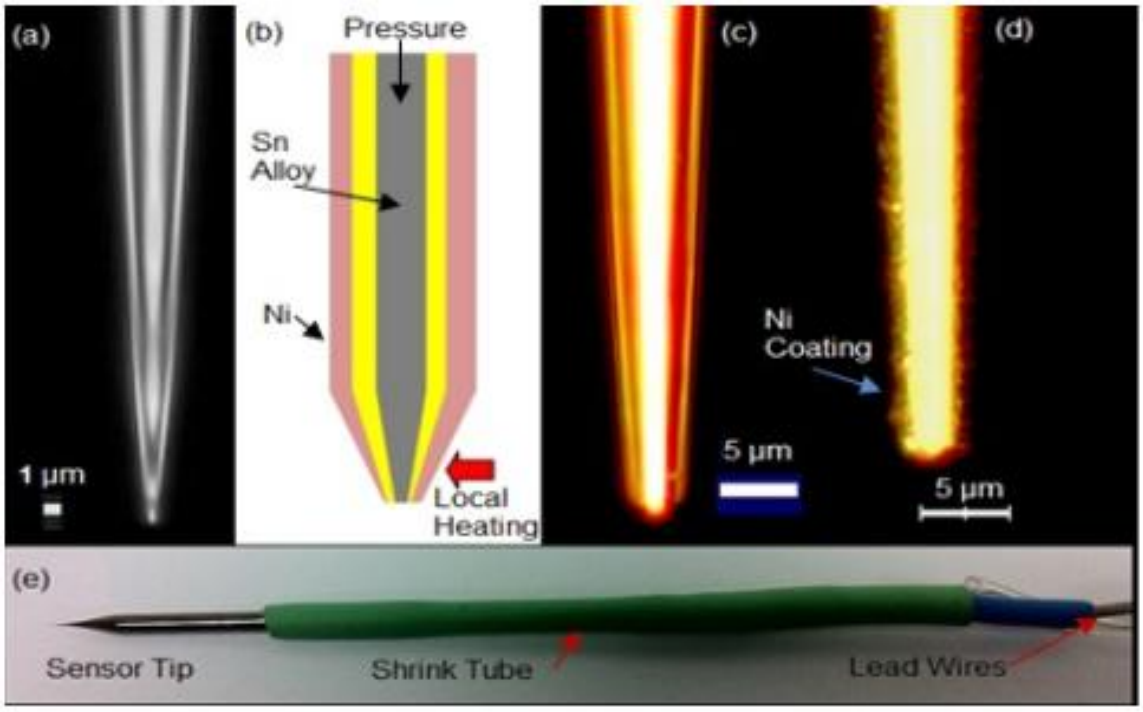

Figure 4.3: Fabrication steps of micropipette thermal sensor: (a) an empty pipette with ~1µm tip opening; (b) a schematic outline of the pipette with a solder alloy inside and nickel coated outside; (c) beveled pipette filled with a solder alloy; (d) pipette with thin film of nickel coated with physical vapor deposition (PVD); (e) a prototype micropipette thermal sensor

4.2.2 Thermocouple Junction between Ni and Solder Alloy at the Tip

The next step is to create a fine thermocouple junction between Ni and solder alloy at the tip of the pulled pipette. The pulled pipette was filled with solder alloy by heating the solder towards the taper end and pressurizing (mechanically) or pushing the other end till the taper was uniformly filled with the solder alloy. The heating temperature was maintained around 300°C with the help of soldering gun.

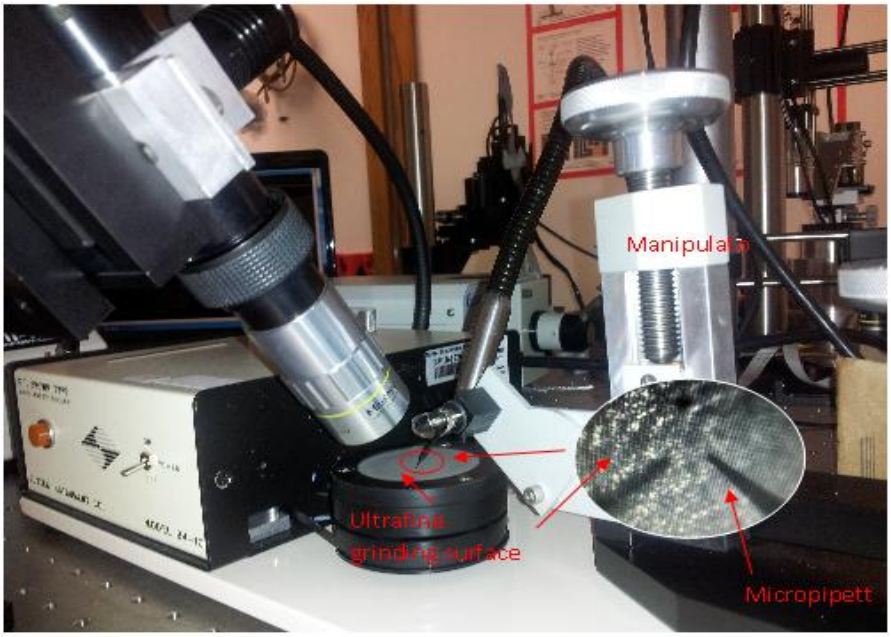

Figure 4.4: Set up used for beveling micropipette using BV-10 micropipette beveler

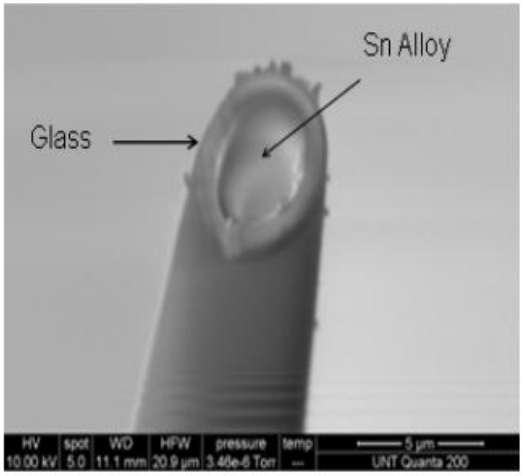

Figure 4.5: SEM image showing the beveled tip of micropipette before Ni deposition

The filled pipette was then beveled using micropipette beveler in order to remove unwanted solder metal extruding from the tip and smoothing the tip surface, so that, a fine and continuous contact can be established when the outer surface of the pipette is coated with Ni. The pipette is beveled using BV-10 micropipette beveler (Sutter Instrument). This beveler was designed for beveling micropipettes with tip diameters between 0.1µm to 50µm. The bevel angle was adjusted in between 25°C to 30°C with the help of X-Y axis micromanipulator that consisted of an angle plate to clamp the pipettes. The pipette was approached towards ultrafine grinding surface (0.3µm alumina abrasive) of beveler with the help of control knobs mounted on the manipulator. The whole process was monitored using a high magnification lens and a Charge Couple Device (CCD) camera from Mightex.

After beveling, the pipettes were cleaned with ethyl alcohol using ultrasonic cleaner (SHARPERTEK). The outer surface of the cleaned pipettes was then coated,

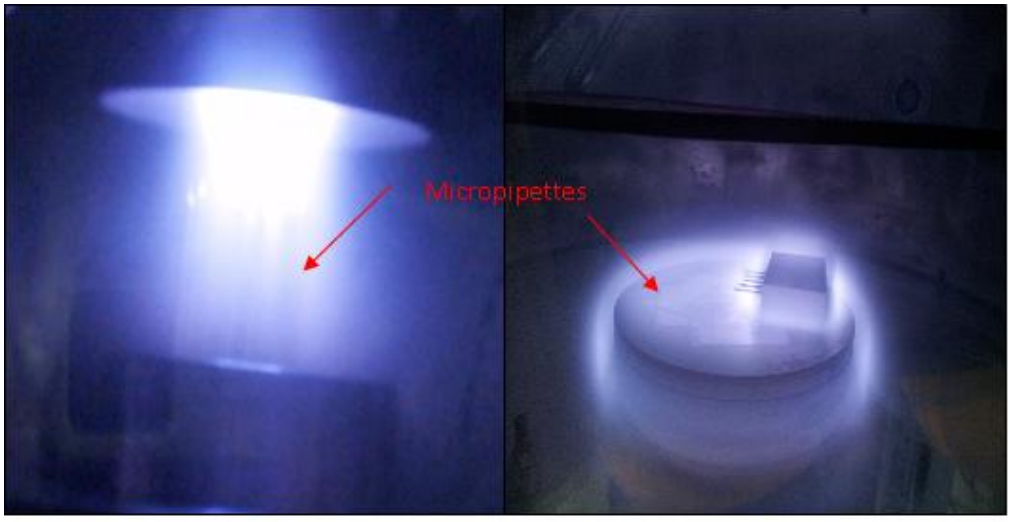

Figure 4.6: Physical vapor deposition (PVD) coating inside the chamber

using physical vapor deposition (PVD) technique, with the thin layer (200nm to 400nm) of Nickel to create a Ni-Sn junction at the beveled tip. The uniform coating of the Nickel

around the tip ensured the quality (sensitivity) of the coated pipette sensors. Nickel vapors were deposited on the outer surface of the pipette under different coating conditions to create a pipette with different sensitivities. Not all of the pipettes with the Nickel deposition worked as sensors. Only the pipettes with a good contact with the Sn alloy at the tip worked as sensors which can be determined by checking the resistance of the Sn-Ni junction at the tip using the voltmeter. The good sensors are then subjected to the calibration.

4.2.3 Calibration

Calibration is the process of determining the sensitivity of the sensor or the Seebeck coefficient of the Sn-Ni junction. So, before using the fabricated sensors for the measurement it needs to be calibrated. The higher the Seebeck coefficient value the greater will be the sensitive of the sensors**.**

Before calibrating, the sensors were wired in order to connect them to the voltmeter. Since, the contact between two different wires would generate a Seebeck voltage the outer surface of the pipette with a Ni coating was wounded by a Ni wire and held firmly with the epoxy, whereas, solder wire was soldered to the inner filled solder. In order to avoid the direct contact of Nickel wire and solder alloy, and to secure the firm and rigid connection between the coated Ni and the Ni wire the heat shrink tubes were used which otherwise would increase the contact resistance and decrease the sensitivity of the sensors.

The calibration of the sensors was done using the thermally insulated cylindrical chamber filled with water. The cylindrical chamber was made of aluminum and insulated from the external environment with the Teflon. The basic concept of the calibration is to

observe the change in the voltage with the change in the temperature of the water i.e. the Seebeck coefficient. Thus, to acquire the best Seebeck coefficient the data were collected only after the water inside the chamber was maintained at constant level with an accuracy of ± 0.1^{o}C. The five sets of data were taken at an interval of 4^{o}C starting at

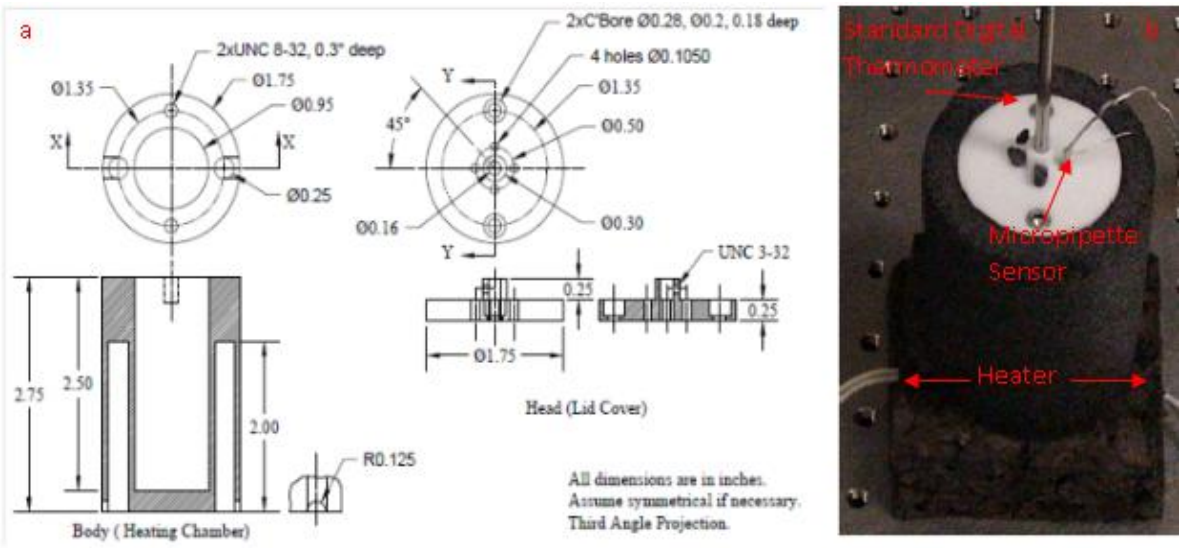

Figure 4.7: (a) Schematic diagram of a calibration chamber; (b) a calibration chamber with insulation

the room temperature. The temperature was varied using an in-house temperature controller integrated with an automated data logging system with LabVIEW. In addition to micropipette sensor, the high precision digital thermometer was immersed next to the sensor inside the aluminum chamber filled with water in order to determine the actual temperature of the water as sensed by the sensor. The voltage was detected by the nano-voltmeter (Keithley 2182) and was recorded using the LabVIEW program for a period of 60 seconds at an interval of every 10 seconds. The two ends (solder and nickel) of the pipettes were connected to the voltmeter with the help of copper wire. Since, the junction between the Sn-Cu and Ni-Cu would generate the unwanted signals the cold junction block was made which would avoid the unwanted signals from

effecting the calibration process. The cold junction block was maintained slightly above the room temperature which was again controlled using the LabVIEW program.

Figure 4.8: LabVIEW program used for controlling the temperature of water bath and cold junction

4.3 Works Cited

1. Volkert, C. A. and A. M. Minor. "Focused Ion Beam Microscopy and Micromachining." *MRS Bulletin* (2007): 389-395.
2. "DualBeam™ Instruments." n.d. *DualBeam (FIB/SEM) Microscopes.* Website. 11 March 2013.

3. Giannuzzi, Lucille A. and Fred A. Stevie. *Introduction to Focued Ion Beams: Instrumentation, Theory, Techniques, and Practice*. New York: Springer, 2005. Print.
4. "Scanning Electron Microscopy (SEM)." Website. 11 March 2013.
5. "Focused Ion Beams." *Focused Ion Beams (FIB) Systems.* Website. 11 March 2013.
6. Orloff, Jon, Lynwood Swanson and Mark William Utlaut. *High Resolution Focused Ion Beams: FIB and its Applications: The Physics of Liquid Metal Ion Sources and Ion Optics and Their Application to Focued Ion Beam Technology*. New York: Kluwer Academic/Plenum, 2003. Print.
7. "The Principles of FIB/SEM Dual Beam Systems." n.d. *Principles of FIB.* Website. 11 March 2013
8. Shrestha, Ramesh. *High-presicion Micropipette Thermal Sensor for Measurement of Thermal Conductivity of Carbon Nanotubes thin film*. Master's Thesis. Denton: Univeristy of North Texas, 2011. Print.

CHAPTER 5

EXPERIMENTAL SETUP AND MEASUREMENTS

In order to determine the thermal conductivity of the materials different variables should be experimentally determined before the theory discussed in chapter 2 can be used. This chapter summarizes the procedure followed to determine different unknown variables and the experiment set up used to calculate the thermal conductivity of the materials.

5.1 Experimental Setup

The schematic drawing of the experimental setup used for the measurement is shown below in figure 5.1. The whole experiment is performed on the smart table so as to avoid any unparallel vibration during the experiment. The setup consists of a laser source, optical devices, a fiber optic illuminator and a charged coupled device (CCD) camera. Laser radiation was produced from the laser source, and this laser radiation was guided and aligned on top surface of the sample with the help of optical devices. An illuminator was used to illuminate the sample while the whole experiment was being monitored with the help of a CCD camera.

A laser source is placed horizontally at the certain height from the surface of the smart table. The laser radiation coming from the source is collimated with the help of the combination of anti reflection coated lenses, so that, the parallel rays of laser radiation propagates towards a beam splitter (position 4 in figure 5.1). These parallel rays of laser get diverted at an angle of 90° at beam splitter (THORLABS CM1-BS013) and forwards towards the sample. The diverted laser then passes through an objective lens (20X Mitutoyo) and gets focused at its focal plane. The focused laser was characterized

based on Gaussian Profile and its diameter was determined to be ~4μm. The focal plane (thus the focal length) of an objective lens was figured out with the distinct image of an object formed with the help of CCD camera.

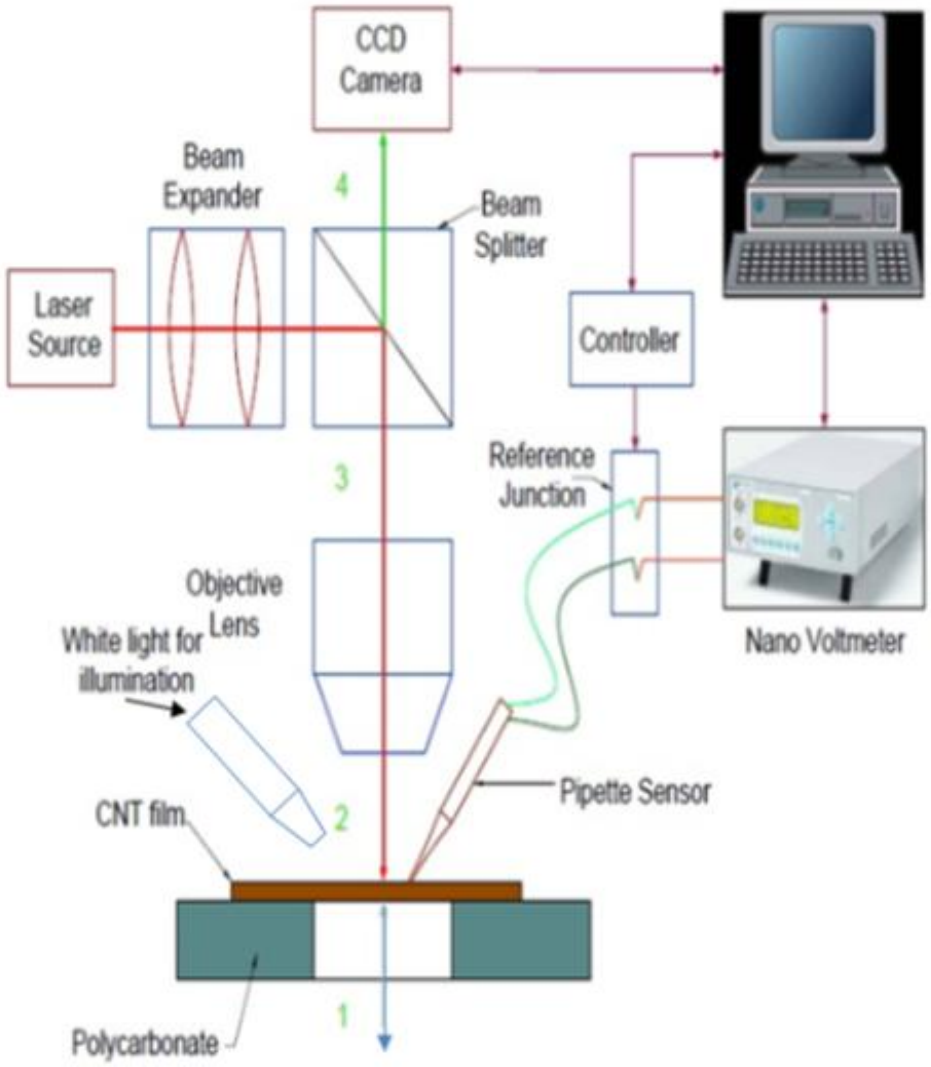

Figure 5.1: Experimental setup used in the measurement

During the experiment the sample was placed horizontally at the focal plane of 20X objective lens and the laser radiation was focused at its center. A white light, guided with a fiber optic illuminator (Edmund optics MI-150), was used to illuminate the surface of the sample. The sample was positioned and aligned with the help of XYZ

motorized stage. Similar motorized stage was used to control the micropipette thermal sensors while approaching and landing on the surface of the sample at different locations.

The power of the incident laser radiation was controlled using a variable neutral density (ND) filter. The power was adjusted in such a way that all the radiation was incident on the surface of the sample. The laser radiation was illuminated at the center of the sample so as to have the uniform heat flow in all the directions. Before the measurement, the nearest possible position of the micropipette sensor tip from the center of the laser spot was determined by checking the effect of the laser radiation on the signal produced by the micropipette sensor. The position was determined by the fact that there is no change in the signal reflected by the micropipette sensor before and after the laser radiation at the particular position. The positioning distance from the center of the laser spot of the micropipette sensor was found to be >6μm. During the measurement the landing of the micropipette sensor was confirmed by careful observation of the live image from the CCD camera. A slight movement or the change in the contrast would confirm that the surface was in contact with the micropipette sensor. Moreover, the change in the signal reflected by the micropipette sensor was used to assure the landing of the pipette sensor. In order to minimize the contact resistance in between the micropipette sensor and the surface of the sample the micropipette sensor was pushed against the surface of the sample further with the help of motorized stage moving 10μm at a time till the voltage reflected by the nanovoltmeter connected to the pipette sensor showed no significant changes after the movement. Thus, the voltage was recorded at this particular position after letting it settle at the steady state for a

certain period of time and the same process was repeated to measure the voltage signals at different position.

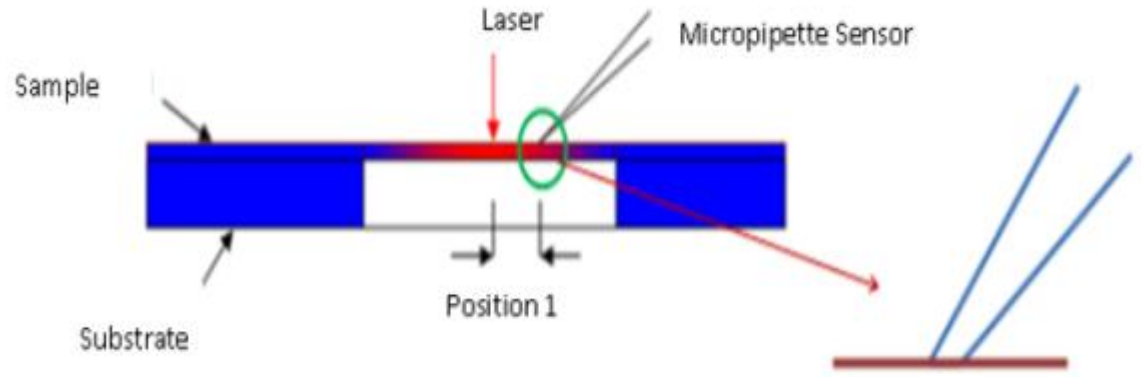

Figure 5.2: Schematic diagram showing the incident laser on the sample and the sensor positioning during the data acquisition

The voltage signal reflected by the nanovoltmeter (Keithley 2182) at the particular position after reaching the steady state was recorded with the help of LabVIEW program. The LabVIEW program recorded the data for the time period of 60 seconds such that for every 10 seconds 3 data were taken and the average of them was returned (similar to the reading taken during the calibration). So, by the end of the experiment I had 6 returns for each position and the average of these data was taken for further calculation. The validity of the data was confirmed by the fact that the voltage signal reflected by the nanovoltmeter was relatively higher when the laser was irradiated and the sensor was touching the surface of the sample compared to the voltage signal reflected when the sensor was not in touch with the surface of the sample. This signifies that the micropipette sensor is actually measuring the signal coming from the surface of the sample. The power setting was unaltered and maintained at the constant level throughout the experiment.

Now with the help of two sets of data from two different positions of the micropipette sensor on the surface of the sample and the known Seebeck coefficient of the used micropipette sensor the temperature difference in between these points can easily be determined using the Seebeck principal.

In order to determine the distance between two positions of the micropipette sensor on the surface of the sample the image taken from the CCD camera was used. The image from the CCD camera was first calibrated with the help of an image taken from the scanning electron microscope (SEM) as shown in the following figure 5.3.

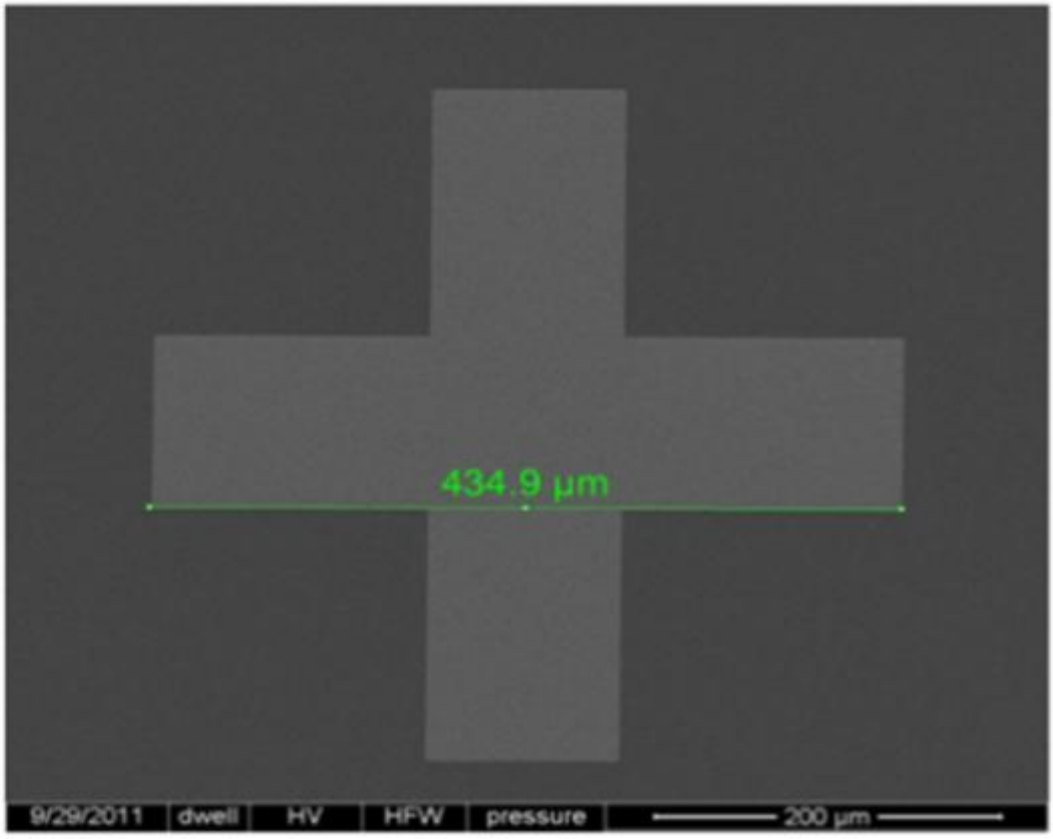

Figure 5.3: SEM image used for the calibration of an image taken from CCD camera

Initially, the number of pixel of a certain known distance of the calibrated image was counted (434.8µm in figure 5.3) and the value of each pixel was determined. The number of pixel counted from the center of the laser spot and to the tip of the

micropipette sensor will then give the distance between them. Figure 5.5 shows the centered laser position and two different measurement positions for the SS 304 stripe and CNT film.

5.2 Laser Power Measurement

For the experiment the laser radiation is used as a source of energy. So, to be able to calculate the thermal conductivity of the measured sample the actual energy of the laser radiation absorbed by the sample needs to be determined. The total energy incident in the sample through the laser radiation will be reflected from the surface of the sample, transmitted through the sample, and absorbed by the sample. In order to determine the thermal conductivity of the sample it is necessary to determine the total energy absorbed by the sample as this is the energy which contributes towards the increase in the temperature of the sample through the heat conduction mechanism. Using the principle of conservation of energy the total power absorbed by the sample was determined, according to which the total laser power incident on the surface of the sample is equal to the sum of power absorbed by the sample (absorptivity), reflected by the sample (reflectivity) and transmitted through the sample (transmissivity) i.e.:

$$\text{Total Inciden Power} = \text{Absorbed} + \text{Transmitted} + \text{Reflected} \qquad (5.2)$$

In other form it can simply be expressed as:

$$Reflectivity\ (R) + Transmissivity\ (T) + Absorptivity\ (A) = 1 \qquad (5.3)$$

In order to determine the total incident power of the laser irradiation on the surface of the sample a digital power meter (THORLABS PM100D) was used. This power meter was connected to the computer where the collected data was recorded. The laser power was measured at four different positions (position 1, 2, 3 and 4 in figure

5.1) for a period of 30 seconds. The following table gives the information on the power measured at different positions.

Table 5.1: Power measured at different position in the experiment and their information

Power Measured at Position	Information
1	Power transmitted through the sample
2	Power incident on the sample
3	Power incident on the objective lens
4	Power reflected

The purpose of the measurement of the power at position 3 and 4 was basically to determine the total power loss in an objective lens and the beam splitter. With an individual measurement of the power of the laser radiation passing through the beam splitter, it was determined that 45% of the power was refracted whereas 55% was reflected. The reflected power at position 4 was mathematically related to the measured power at the same position (P_4) through the following expression which accounts for the total loss of power in an objective lens and beam splitter.

$$P_4 = [\{R - (R \times \%\ \text{loss in an objective lens})\} \times 0.45] - [\{R - (R \times \%\ \text{loss in an objective lens}\} \times \%\ \text{loss in a beam splitter} \quad (5.4)$$

Equation 5.4 helps to calculate the total power reflected from the surface of the sample. So, with the calculated power at position 4 (reflected power), measured power at position 1 (transmitted power) and position 2 (incident power) the total power absorbed by the sample can be calculated easily using equation 5.2.

5.3 CNT Thickness Measurement

The thickness of the CNTs film was determined with the magnified SEM image of the CNTs. The CNTs film was poked and damaged so as to make the lateral part, which gives the thickness, of the film visible. It was aligned vertically in such a way that the microscope was directed straight towards the lateral part. Hence, the thickness was measured. Images for four different CNT films used in the research are shown in figure 5.4 in an increasing order.

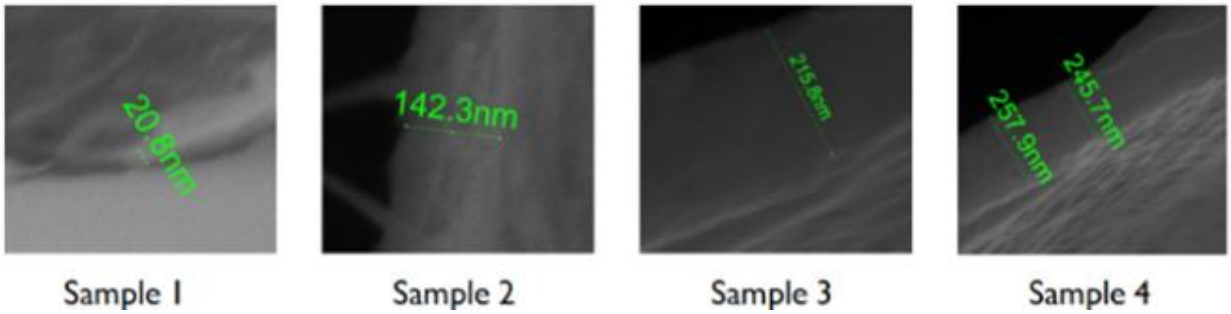

Figure 5.4: SEM images showing the thickness of CNT films

After all the parameters required for the measurement were completed, the Fourier law for one dimensional heat diffusion given by equation 2.2 was used for the calculation of the thermal conductivity of the stainless and the radial heal flow conduction given by equation 3.1 was used for the calculation of the thermal conductivity of the CNT films.

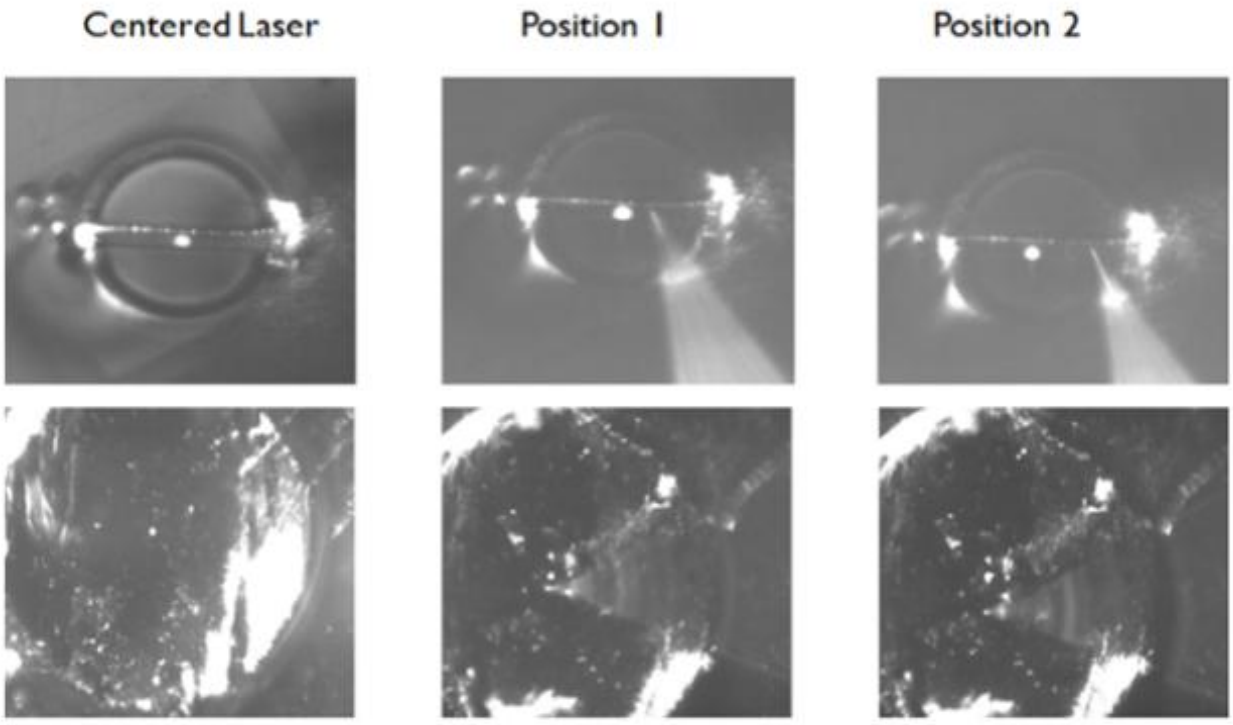

Figure 5.5: SS 304 stripe (top) and CNT film (bottom) showing the centered laser spot and two different positions used during the measurement

5.4 Works Cited

1. Van-Herwaarden, A. W. and P. M. Sarro. "Thermal Sensors Based on the Seebeck Effect." *Sensors and Actuators* (1986): 321-346. Print.
2. Molki, Arman. "Simple Demonstration of the Seebeck Effect." *Science Education Review* (2010): 103-107. Print.
3. Shrestha, Ramesh. *High-presicion Micropipette Thermal Sensor for Measurement of Thermal Conductivity of Carbon Nanotubes thin film*. Master's Thesis. Denton: Univeristy of North Texas, 2011. Print.

CHAPTER 6

RESULTS AND DISCUSSIONS

This chapter summarizes the result and conclusion drawn after performing series of experiments. The chapter starts with the calibration of the pipettes used for the experiments. The result of the behavior of the same pipette and batches of pipette from the same Nickel film coating conditions are discussed. The measurement for the CNT films and stainless steel stripe (304) using the pipette sensor is then summarized and the simulation result for the SS Stripe (304) is presented. Finally, the reliability and durability test result is summarized under different performed conditions.

6.1 Calibration of Pipette Sensor

Calibration of the micropipette thermal sensors is done to figure out the Seebeck coefficient of the thermocouple junction formed at the tip of the micropipette sensor. Only after the calibration of the micropipette sensors it is possible to know and relate the temperature of the measured sample via the voltage reading through the sensor. It is a very crucial part during the fabrication of the micropipette sensor as an error made during this process will result in the meaningless measurement of the samples made with the micropipette sensor.

A comprehensive study on the behavior of the micropipette sensors based on the different physical vapor deposition (PVD) setting used during the Nickel film coating is done. At first the Seebeck coefficient of the pipettes with different tip sizes but coated together under same circumstances are compared. The comparison is done for two batches of micropipette sensors with two different PVD settings. The study in the behavior of the same pipette was performed by repeating the calibration so as to see

any fluctuations in the calibrated data. Table 6.1 gives the information on two batches of pipettes coated under different PVD setting. The data reflect that for the pipettes coated under same PVD setting the maximum deviation in the Seebeck coefficient is 0.11. This concludes that the tip size doesn't play significant role in determining the Seebeck coefficient unless the coating setting remains the same.

Table 6.1: Study of the fabricated micropipette sensors for two different PVD settings

Sensor No.	Tip Size (µm)	Seebeck Coefficient(µV/ ^{o}C)	Average Seebeck Coefficient (µV/ ^{o}C)	Standard Deviation
PVD Setting 1				
1	2	7.162	7.229	0.11
2	3.5	7.171		
3	6.5	7.356		
PVD Setting 2				
4	1.9	5.155	5.192	0.10
5	2	5.115		
6	2.5	5.305		

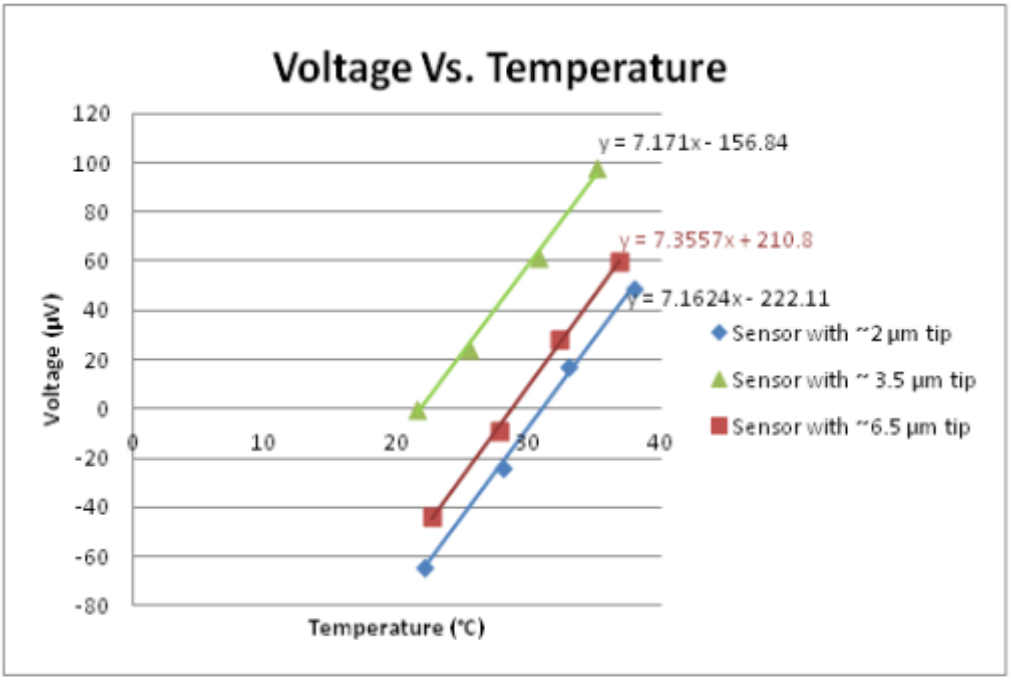

Figure 6.1: Voltage vs. temperature plot for batch of pipettes coated with Nickel film under PVD setting 1

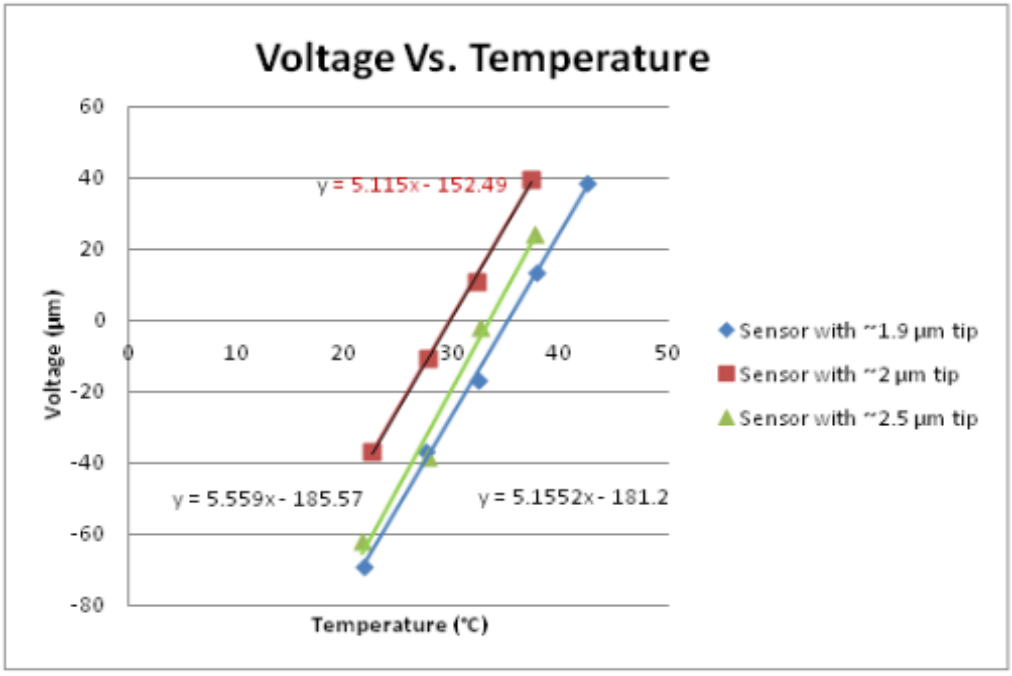

Figure 6.2: Voltage vs. temperature plot for batch of pipettes coated with Nickel film under PVD setting 2

After the study of the behavior of the pipette coming from the same batch of Nickel coating, the behavior of a single pipette was studied so as to confirm that the Seebeck coefficient determined for the pipette is a reliable data. In order to confirm the reliability of the Seebeck coefficient, the same micropipette sensor was calibrated repeatedly. Table 6.2 reflects the results of the repeated calibration for the micropipette sensor of tip size 2.4µm. The standard deviation shown for the three sets of data by the micropipette sensor is 0.09, which is close to the maximum deviation of 0.11 shown by the pipettes from the same batch of Nickel coating. Hence, it can be concluded that for the pipettes coated under same circumstance of the PVD setting the Seebeck coefficient for the pipettes remain almost same without being affected by the tip size.

Table 6.2: Repeated study of the fabricated micropipette sensors

Tip Size (µm)	Calibration No.	Seebeck Coefficient (µV/ ^{o}C)	Average Seebeck Coefficient (µV/ ^{o}C)	Standard Deviation
2.4	1	6.809	6.725	0.09
	2	6.626		
	3	6.741		

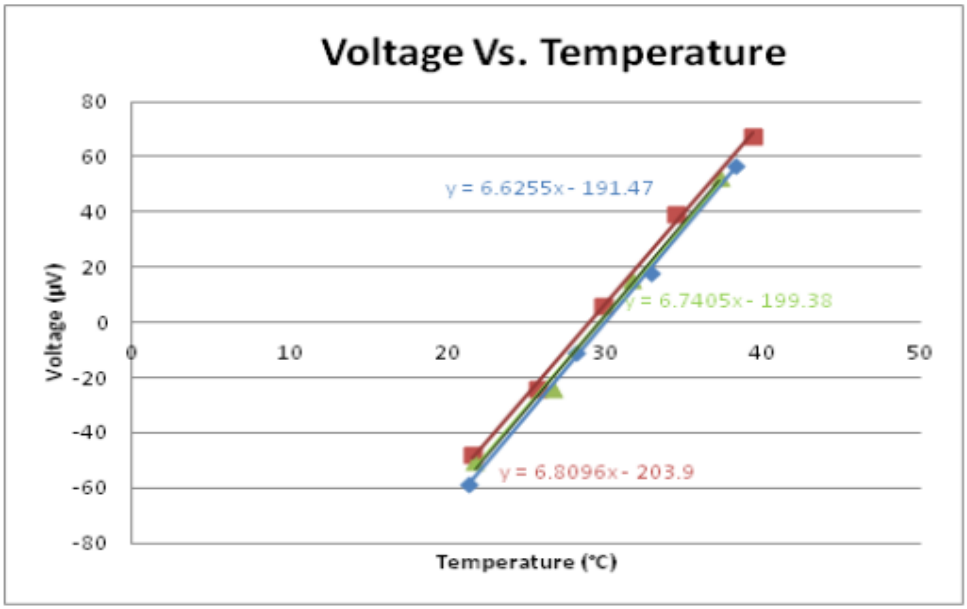

Figure 6.3: Voltage vs. temperature plot for a single pipette for a repeated study of the Seebeck coefficient

The measured Seebeck coefficients value of the sensors is comparatively less than the value of bulk material. The possible reason for this can be related with the thermoelectric behavior of vapor deposited thin metal films [1]. The relation between the thermoelectric power and free electron energy in crystal lattice is given by Hill et al. as

$$S = \frac{\pi^2 K^2 T}{3e\varsigma}\left\{\frac{d\ln\lambda(E)}{d\ln(E)}\right\}_{E=\varsigma} \qquad 6.1$$

Where, S = Thermoelectric power

K = Boltzmann constant

e= Electron Charge

T = Temperature

ζ= Fermi energy

λ = Mean free path of electron

E= Energy of an electron

The Fermi level energy and the mean free path of an electron are affected by the presence of impurities and the thickness of the thin film. They tend to reduce the mean free path and electrical conductivity. Decrease in the mean free path of an electron affects the thermoelectric power as per the relation shown by equation 6.1 which in turn reduces the Seebeck coefficient. The thickness of the coated Ni film is around 300nm – 400nm, and at this thickness level there is the probability of the formation of large number holes or spaces [2] which might either be empty or filled with impurities and defects.

6.2 Thermal Conductivity Measurement of CNT films

Table 6.3 summarizes the detail information on the result obtained for the thermal conductivity of four different CNT films of different thickness. The sensors used for the measurement were from the same batch of nickel coating whose Seebeck coefficient was determined to be 6.877 W/m-K.

During the experiment the laser power was irradiated at the center on the surface of the CNT film. The experiment set up was allowed to settle and reach the steady state before the measurement was taken. Throughout the period of measurement (for one run) the power was maintained at the constant level. The laser power at four different positions as shown in figure 5.1 was measured with the help of power meter to determine the power absorbed by the CNT films. Using these measured power and equation 5.2 the total power absorbed by the sample was calculated. This was repeated for each sample of CNT films. With the power measurement at four different locations as shown in figure 5.1 for all four samples it was concluded that the reflected power remained almost the same for all four samples but there was change in the transmitted

and the absorbed power. The power absorption for the thicker sample was more and the power transmission was less. Now, with the known value of the absorbed power, temperature difference in between two radial positions, distance in between two radial positions, and the thickness of the CNT film the thermal conductivity of the film was calculated using equation no. 3.1. The procedure was repeated again for different power settings and the thermal conductivity value was calculated. This was done for all the four different samples of CNT films and the average thermal conductivity value was taken as a final result for each sample of CNT films. Figure 6.4 gives the information in the thermal transport behavior of CNT films of varying thickness. From this figure it can be concluded that with the increasing thickness of the CNT films the thermal conductivity decreases. The reason for this behavior can be explained by the relation shown by equation 6.2.

$$k = \left(\frac{1}{3} C_v \lambda \right) \tag{6.2}$$

where C_v = Specific Heat

λ = Mean free path

k = Thermal Conductivity

The equation shows a direct relation in between thermal conductivity and the mean free path of an electron. The typical range of mean free path of an electron is in the range of 100nm to 1µm. The thicker sample has a higher density of CNTs and higher degree of tangling which tends to reduce the mean free path and in turn reducing the thermal conductivity of the CNT films.

The heat transfer mechanism happens through the conduction, convection and radiation. The calculation done above is solely based on the conduction mechanism. The heat transfer through the natural convection and the radiation were ignored as they had negligible effect. The percent of heat transfer through the natural convection and radiation was determined to be 0.38% and 0.10% using equation 2.4 and 2.9 respectively.

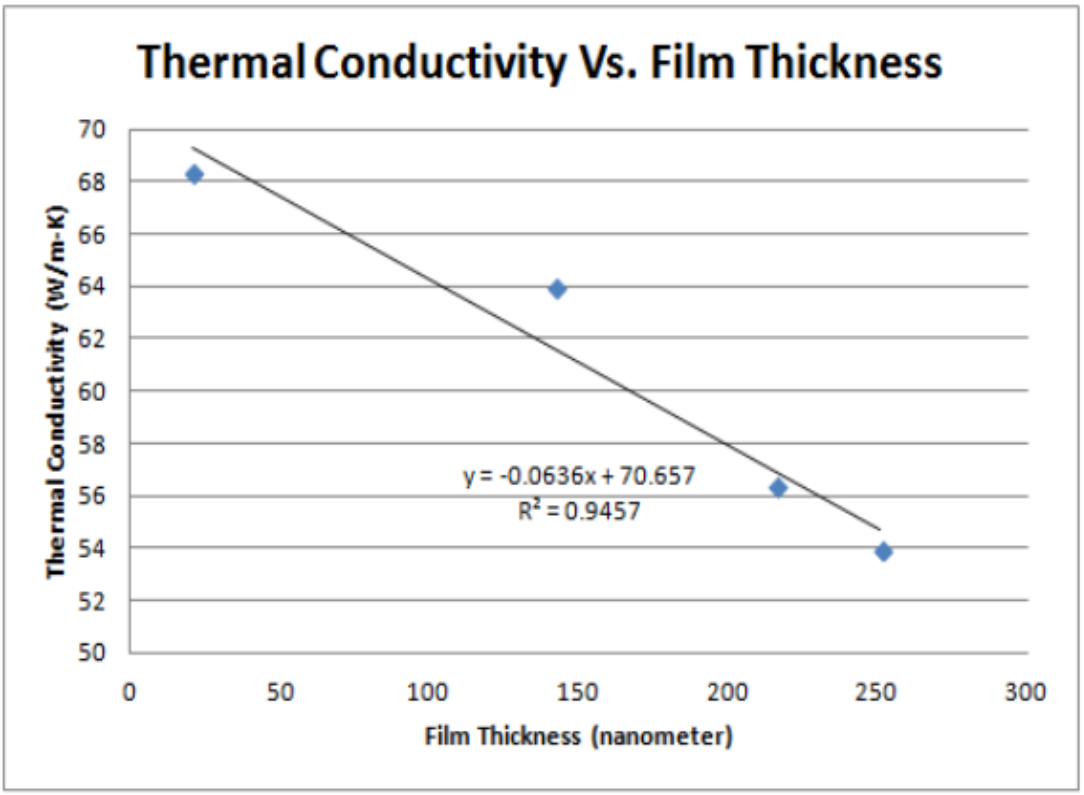

Figure 6.4: Thermal conductivity vs. CNT film thickness plot for comparative study

Table 6.3: Thermal conductivity measurement summary for CNT films

Power Absorbed	Radius 1	Radius 2	Temperature Difference	Thickness	Thermal Conductivity	Average	Standard Deviation
Film Thickness: 21 nanometers							
4.36E-05	45.360	33.166	1.540	2.10E-08	67.245	68.309	1.74
4.36E-05	45.360	40.526	0.530	2.10E-08	70.313		
4.36E-05	40.526	33.166	0.984	2.10E-08	67.370		
Film Thickness: 142 nanometers							
8.63E-05	23.640	10.933	1.183	1.42E-07	63.027	63.930	1.05
8.63E-05	12.456	7.034	0.867	1.42E-07	63.687		
8.63E-05	17.034	8.093	1.106	1.42E-07	65.077		
Film Thickness: 216 nanometers							
7.93E-05	48.026	23.933	0.730	2.16E-07	55.713	56.453	0.68
7.93E-05	50.650	17.280	1.101	2.16E-07	57.048		
7.74E-05	29.342	19.195	0.428	2.16E-07	56.597		
Film Thickness: 251 nanometers							
1.04E-04	15.750	39.140	1.093	2.51E-07	54.778	53.794	0.88
6.34E-05	23.920	56.580	0.647	2.51E-07	53.533		
5.28E-05	35.290	95.350	0.627	2.51E-07	53.070		

6.3 Thermal Conductivity Measurement of the Austenite Stainless Steel

Table 6.4 and 6.5 summarizes the data for the thermal conductivity measurement of the austenite stainless steel. Table 6.4 present the data for the temperature greater than 0.152^{o}C and Table 6.5 present the data for the temperature greater than 0.4^{o}C. The sensors used for the measurement were from the same batch of nickel coating whose Seebeck coefficient was determined to be 6.877 W/mK.

Experiment measurement was carried out when the steady state was reached after the irradiation of the laser power. Measurement was done in four different power settings so as to give different amount of heat energy. Throughout the period of measurement (for one run) the power level was maintained at constant level. The laser power at four different positions show in figure 5.1 was measured with the help of power meter to determine the power absorbed by the stainless stripe. Using these measured power and equation 5.2 the total power absorbed by the sample was calculated. For the particular sample of stainless stripe, out of total power incident on the surface, 61.32% of the power gets reflected, 0.96% of the power gets refracted, and the remaining 37.72% of the power gets absorbed by the stripe. Now, with the known value of the absorbed power, temperature difference in between two positions, distance in between two positions, and the cross section area of the stripe, the thermal conductivity of the stripe was calculated using equation 2.2. The procedure was repeated again for different power setting and the thermal conductivity value was calculated. The averages of all the calculated thermal conductivity value was determined to be 16.39 W/m-K with a standard deviation of 1.39 giving an error of 8.48%. But if the data for the positions where the temperature difference is greater than 0.4°C is considered then the value of

the thermal conductivity will be 15.60 W/m-K with a standard deviation of 0.81 giving an error of 5.19%. From this it can be concluded that higher the temperature difference between the measured positions the better will be the precision of the taken data.

From the literature review it was found that the thermal conductivity of the type 304 stainless steel is 16.2 W/m-K at 100ºC and 21.4 W/m-K at 500 ºC. This value is close to the calculated value for the stainless steel sample. The calculated value of the sample was also compared with the simulation result using Comsol 3.5a, according to which the thermal conductivity of the stripe was determined to be 14.9 W/m-K. Looking at the trend of literature value the thermal conductivity measured can be justified as the thermal conductivity measurement was done at room temperature.

The heat transfer mechanism happens through the conduction, convection and radiation. The calculation done above is solely based on the conduction mechanism. The heat transfer through the natural convection and the radiation were ignored as they had negligible effect. The percent of heat transfer through convection and radiation was determined to be 0.21% and 0.33% using equation 2.4 and 2.9 respectively.

Table 6.4: Summary of the thermal conductivity measurement of the stainless steel

Seebeck Coefficient of the Sensor (µV/ ^{o}C)	Laser Power Incident on the Sample (µW)	Power Absorbed (µW)	P1 (µm)	P2 (µm)	Temperature Difference	Thermal Conductivity (W/m°C)	Mean Thermal Conductivity (W/m°C)	Standard Deviation	Error %
6.877	42.42	16.00	12.52	19.03	0.47	14.76	16.39	1.39	8.48
	42.42	16.00	17.48	10.12	0.80	16.72			
	5.06	1.91	8.97	17.71	0.15	15.54			
	5.06	1.91	8.97	22.54	0.20	18.48			
	43.54	16.42	12.88	15.64	0.40	15.46			
	43.54	16.42	10.81	15.64	0.70	15.46			
	2.99	1.13	7.92	10.56	0.062	17.88			

Table 6.5: Summary of the thermal conductivity measurement of the stainless steel for temperature difference greater than 0.4 °C at two different positions

Seebeck Coefficient of the Sensor (µV/ °C)	Laser Power Incident on the Sample (µW)	Power Absorbed (µW)	P1 (µm)	P2 (µm)	Temperature Difference	Thermal Conductivity (W/m°C)	Mean Thermal Conductivity (W/m°C)	Standard Deviation	Error %
6.877	42.42	16	12.52	19.03	0.47	14.77	15.60	0.81	5.19
	42.42	16	17.48	10.12	0.80	16.72			
	43.54	16.42	12.88	15.64	0.40	15.46			
	43.54	16.42	10.81	15.64	0.70	15.46			

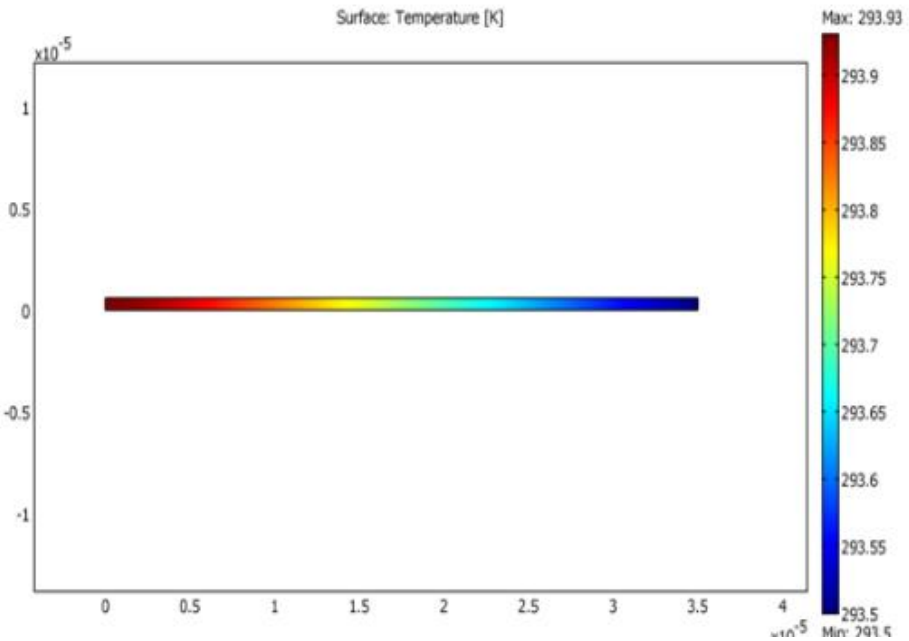

Figure 6.5: Simulation result for the stainless steel stripe (304)

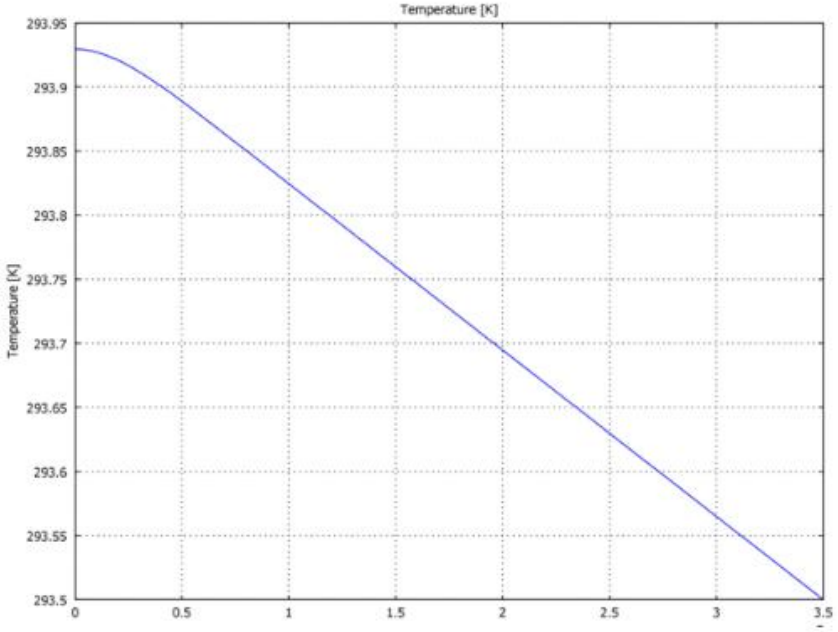

Figure 6.6: Simulated temperature profile along the surface of the stainless steel stripe (304)

6.4 Improvement in the Reliability and Durability of the Micropipette Sensors

During the measurement of the SS 304 stripe it was noticed that the micropipette thermal sensors were dying more frequently. Moreover, I also needed to calibrate the micropipette thermal sensors after it was used for taking couple of data. The reason for this behavior of the pipette was due to the loose contact at the tip where the thermocouple junction was created. The Nickel film was being depleted at the Ni-Sn junction slowly after each use which eventually made the sensors useless. The depletion in the Ni film was due to the galling effect on the rough surface of the SS 304 stripe and the skidding of the micropipette sensors. As the pipette sensor approached the sample at an angle it tends to skid 1µm - 2µm which also contributed in the depletion of the coated Nickel film and eventually leading the sensor to the die. This tendency of depletion of the Ni film effects the reliability in the data taken from the pipette sensor and the durability of the pipette sensor. Moreover, there is a need for calibration of the pipette sensor after running each experiment. In order to avoid this I came up with three different solutions: annealing, rubber coating at the tip and bending tip at the taper.

6.4.1 Annealing

Annealing treatment helps in the re-crystallization of the grains and increases its size reducing defects like dislocations. It reduces the thermal stress which benefits the heat conduction and thus improves the thermal conductivity. The annealing of the pipette sensor was done at 100°C as the melting point of the solder alloy was around 110°C.

6.4.2 Rubber Coating at the Tip

Rubbers are tough polymeric substance which are made from the latex of tropical plants or synthetically. They are elastic, tough, adhesive, impermeable, and non conductor. These properties of the rubber make it the solution to the problem of the depletion of micro pipette sensors. Coating the rubber at the tip helps to protect the coated Ni film from being depleted. For coating the micro pipette sensors a poly glass rub 50 RTV liquid rubber and silicone rubber were used. Poly glass rub 59 RTV liquid rubber consisted of two parts A and B. Two parts were taken in equal volume and mixed firmly. The mixed rubber was subjected to vacuum degassing to get rid of air bubbles. The mixed rubber was then applied to the pipette sensor and cured at room temperature to get the uniform flexible clear rubber.

6.4.3 Bending Tip at the Taper

Bending pipette at the tip is another solution concerning reliability issue. The skidding problem of the pipette sensor is due to an angle at which it is approached to the sample. Bending the pipette tip at an angle in such a way that the approach angle to the sample is close to 90º will help to prevent the skidding problem and thus the depletion of the coated nickel.

Figure 6.7: Sensor with bent tip

6.5 Calibration of Rubber Coated Pipettes

One of the objectives of this thesis is to increase the reliability and durability of the existing micropipette sensors through rubber coating. The reliability and the durability of the sensor were being affected by the galling effect. Galling is a form of wear which is caused by adhesion between the sliding surfaces. When the pipette lands on the surface of the sample the nickel film galls due to which some of it is pulled with the contacting surface. It is caused by friction and adhesion between the sensor tip and the surface of the sample which is followed by the slipping and tearing.

The result for the calibration of the three different micropipette sensors before and after the rubber coating is summarized below in Table 6.6. All the three pipettes considered for the study has different tip sizes and the Seebeck coefficient. All three pipettes were rubber coated under the same circumstances and were given same amount of curing time (24 hours).

Table 6.6: Study of fabricated micropipette sensors before and after rubber coating

Sensor No.	Tip Size (µm)	Seebeck Coefficient (µV/ ^{o}C)		
		Before	After	Difference
1	2.1	8.9016	7.2712	1.6304
2	3.3	7.5418	6.2346	1.3072
3	6.5	7.3557	6.7405	0.6152

In the data from Table 6.6, it clearly shows that the Seebeck coefficient of the sensors decreases after the rubber coating which is due to the characteristic property of the rubber. Rubber is a bad conductor of electricity, thus the heat, with the thermal

conductivity value ranging from 0.09 – 2.31 W/m-K based on the nature of rubber. Moreover, the shrinkage of the rubber, after it is cured, tends to build up the pressure at the interface between the solder metal and the nickel film which tends to loosen the contact in between the solder alloy and Nickel film and, thus, decrease the sensitivity. Further analysis in the nature of reduction of the Seebeck coefficient shows that the smaller tip sized sensors have the higher reduction in the Seebeck coefficient compared to the bigger tip.

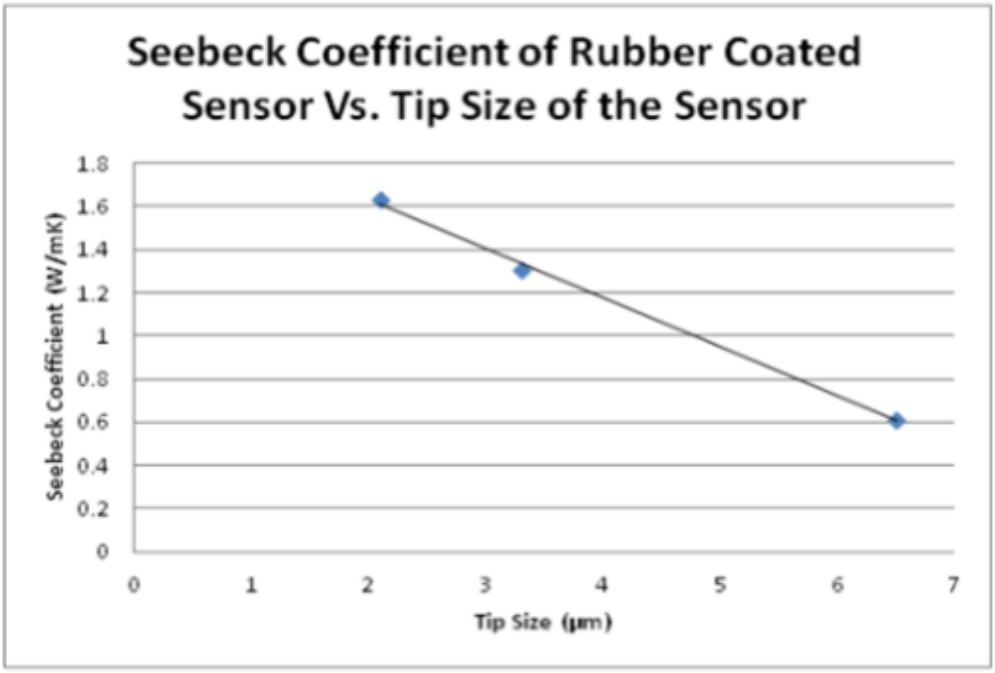

Figure 6.8: Seebeck coefficient vs. tip size plot for rubber coated micropipette thermal sensors

6.5.1 Reliability Test

The reliability test for the micropipette sensors were done under different conditions. The reliability was checked through annealing, rubber coating and landing position of the pipette sensor. The figure 6.9 gives the comparative study on the effect

of different steps undertaken to improve the reliability and durability of the pipette sensor. The reliability test for the pipettes was done by repeatedly landing the pipette sensor on the surface of the silicon. After the repeated landing of the pipette it was then calibrated to see the change in the Seebeck coefficient. Table 6.7 through 6.9 summarizes the information on the reliability test done for micropipette sensors treated under different conditions.

Table 6.7: Study of the sensitivity of a sensor before and after reliability teat at an angle

No. of repetition	Tip Size (µm)	Seebeck Coefficient (W/m.K)			% Change after 100 repetition	% Change after 1 repetition
		Before	After	Difference		
100	2.4	6.6255	5.7881	0.8374	12.63	0.1263
			5.7511	0.8744	13.19	0.1319

Table 6.8: Study of the sensitivity of a sensor before and after vertical reliability test

No. of repetition	Tip Size (µm)	Seebeck Coefficient (W/m.K)			% Change after 100 repetition	% Change after 1 repetition
		Before	After	Difference		
100	2.1	5.6364	5.1145	0.5219	9.26	.0926

Table 6.9: Study of the sensitivity for an annealed sensor before and after vertical reliability rest

No. of repetition	Tip Size (µm)	Seebeck Coefficient (W/m.K)			% Change after 100 repetition	% Change after 1 repetition
		Before	After	Difference		
100	2.1	7.0305	6.7336	0.2969	4.22	.0422

There was change in the sensitivity of the pipette after the reliability test. The reason behind this can be attributed to the mechanical stress at the tip of the pipette during the landing and leaving the surface of the sample. Moreover, the annealed pipette sensors landing vertically showed the better result in the improvement of the reliability and durability of the micropipette sensors. The percent change after each repetition for the annealed sensor when tested vertically showed the 0.0422% change. Thus, it can be concluded that by annealing pipette and approaching the surface of the sample vertically improved the life of the micropipette sensors.

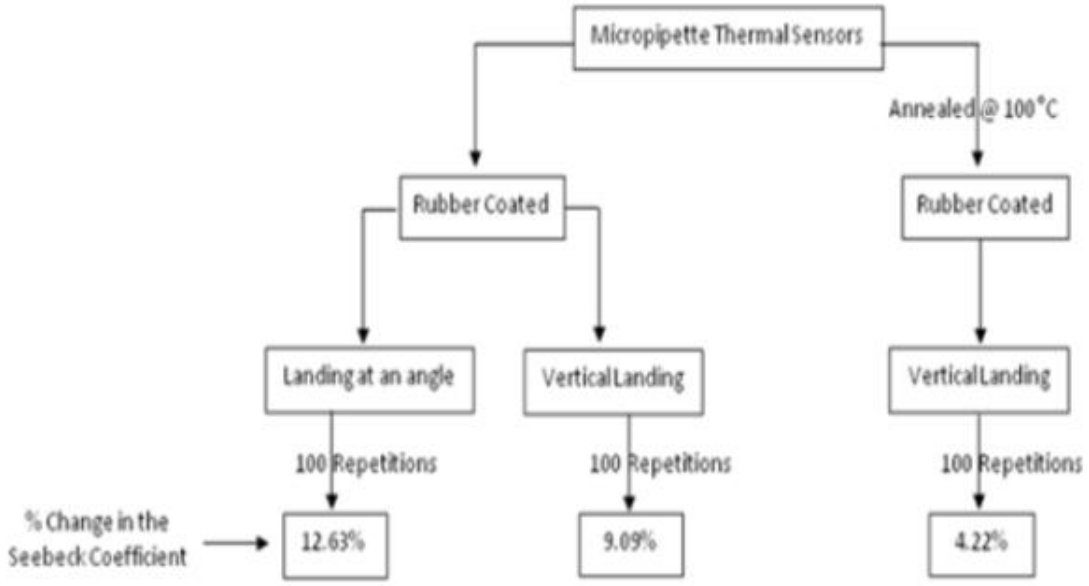

Figure 6.9: Flow diagram summarizing the reliability test and its result

The micropipette sensors were annealed at only 100°C. There was a constraint to anneal the temperature at higher temperature as the melting temperature of the solder alloy is 129°C. Increasing the temperature would, thus, melt the solder which in turn destroys the solder-nickel junction eventually making the sensor useless.

6.6 Works Cited

[1] Hill, D. E., et al. "The effect of physical vapor deposition parameters on the thermoelectric power of thin film Molybdenum-Nickel junctions." *Thin Solid Films* (1997): 263-270.

[2] Adamov, M., B. Perovic and T. Nenadovic. "Electrical and structural properties of thin gold films obtained by vacuum evaporation and sputtering." *Thin Solid Films* (1974): 89-100.

CHAPTER 7

CONCLUSIONS AND FUTURE WORKS

7.1 Conclusions

A micropipette thermal sensor was fabricated based on the thermocouple principle with the tip size of around ~2 µm. The fabricated sensors were calibrated to determine its sensitivity (Seebeck coefficient) and were used for thermal characterization of CNT films and austenite stainless stripe (304). During the calibration of the micropipette sensors it was determined that for the same batch of the pipette undergoing the Ni coating in the PVD, the sensitivity of the micropipette sensors deviated by 0.11 without being affected by the tip sizes of the pipettes. Also, the repeated calibration of a micropipette showed the deviation of 0.09 in the sensitivity.

CNT films of different thickness were thermally characterized using the fabricated micropipette thermal sensors. The thickness of the CNT films affected the amount of laser power being absorbed by the film. The increasing thickness tends to absorb more power while decreasing the amount of power transmitted through it. The thermal conductivity of the CNT films showed the inverse relation with the thickness of the CNT films i.e. thicker the films lower the thermal conductivity.

Austenite stainless steel (304) was thermally characterized using the micropipette sensor. The experimentally determined thermal conductivity value of the SS 304 stripe at room temperature for all temperature range was 16.39 ± 1.39 W/m-K. Further analysis of the data by considering the higher temperature difference between the two positions being considered gave the value of 15.60 ± 0.81 W/m-K which has more precision. Hence, it can be concluded that greater the temperature difference

between two positions better precision the data obtained. During the measurement of SS 204 stripe the change in the sensitivity of the micropipette sensors was noticed which was because of the wearing of the nickel film due to galling and sliding of the micropipette sensor. In order to avoid the galling and sliding of the micropipette the micropipettes were annealed and rubber coated. The reliability test performed for the micropipette sensors based on an angle of approach towards the sample concluded that the vertical landing was effective compared to the landing at angle. Also, the annealed pipette showed the effective improvement over the pipette without annealing. The change in the sensitivity for the annealed and rubber coated pipette approaching the surface of the silicone vertically was determined to be 4.22% after 100 repetitions.

7.2 Future Works

Future work will possibly take the following steps for the further study

- Improving the reliability of the micropipette sensors using the following alternatives:
    - Improving annealing temperature of the sensors by using solder metal with high melting point
    - New method to insert the high melting point solder without destroying tip
    - Alternative coating using alumina, diamond like carbon (DLC) etc.
- Thermal characterization of the Stainless Stripe after ion irradiation